Whole-Body Chemiluminescence and Fluorescence Imaging of Inflammation

Jen-Chieh Tseng and Jeffrey D. Peterson

Abstract This chapter focuses on the application of optical imaging methods to visualize inflammation in living animals. Optical imaging has several advantages as it operates without any involvement of ionizing radiation or strong magnetic fields. Optical imaging uses nonradioactive probes that produce chemiluminescent or fluorescent light signals in the visible, far-red, or near-infrared (NIR) range of the electromagnetic spectrum. To visualize inflammation at the tissue level, high molecular weight probes can be used to produce fluorescent contrast in the inflamed tissues by taking advantage of the enhanced permeability and retention (EPR) effect. In addition to this general, but rather less selective, approach, the chapter discusses the more specific and mechanistic imaging strategies that specifically target several unique biological aspects of inflammatory processes at the cellular and enzyme levels. These unique aspects include the inflammatory phagocytes that produce reactive oxygen species (ROS), and the tissue-remodeling proteases present in the inflamed tissues. Once activated, specific probes can produce visible or NIR luminescent signals that can be quantified for assessing inflammatory responses. Although visible light is subject to scattering and attenuation in the tissue, fluorescent probes that use NIR light sources have improved tissue penetration allowing generation of 3D tomographic images.

Keywords Inflammation · Chemiluminescence · Fluorescence · Inflammatory phagocytes · Reactive oxygen species (ROS)

J.-C. Tseng (✉) · J. D. Peterson
PerkinElmer, Inc., Hopkinton, MA, USA
e-mail: jen-chieh.tseng@perkinelmer.com

F. Man, S. J. Cleary (eds.), *Imaging Inflammation*, Progress in Inflammation Research 91, https://doi.org/10.1007/978-3-031-23661-7_5

1 Introduction and Background

1.1 Significance of Imaging Inflammation in Animal Models

Inflammation is a fundamental biological aspect of many human diseases. It is the body's natural defense mechanism in response to physical damage, microbial infection, and other tissue insults [1]. In addition, inflammatory processes are known to be associated with various noninfectious pathological conditions such as cancer [2] and neurodegenerative diseases [3]. Although ubiquitously observed in many human diseases, inflammation is an intricate and highly regulated dynamic process that evolves over time, involving the collaboration of many different types of cells. The process typically begins with resolving microbial infection and clearance of damaged tissue and cell debris at early stages. The goals of inflammation later shift to promoting tissue regeneration, restructure, and its eventual repair. As inflammation is an intricate, dynamic, and collective phenomenon involving many cellular players, it is virtually impossible to study inflammation without the use of living subjects as research models. Animal inflammation models provide closer representations of human diseases, and noninvasive molecular imaging provides a means to follow the dynamic changes in target tissues.

Molecular imaging methods that specifically target cells that drive inflammatory responses can be very useful for inflammation research, but the selection of effective imaging strategies requires extensive knowledge of inflammation biology. Several types of immune cells are involved in inflammation and, among them, phagocytes are particularly important during tissue inflammatory responses. These specialized leukocytes include granulated neutrophils, phagocytic monocytes, and macrophages. All three cell types are considered major professional phagocytic cells for their unique capability to engulf and digest invading microbes or tissue debris. In addition to their phagocytic capability, each of these cell types is equipped with specific enzymatic tools to exert their necessary inflammatory functions at different stages of inflammation. These unique enzymatic tools can also help them communicate and coordinate with other immune and somatic cells to achieve their inflammation-specific objectives. Since tissue inflammation is largely mediated by neutrophils and monocytes/macrophages, many inflammatory imaging methods have been developed by specifically targeting these phagocytes. This review will begin with an in-depth discussion of critical cellular players in inflammation and the proteases, enzymes, and other factors important in their inflammatory effector functions. The attention will then focus on recent noninvasive chemiluminescence imaging (CLI) and fluorescence imaging (FLI) strategies that exploit these unique inflammatory features and functions for noninvasive, real-time assessment of inflammation and treatment.

1.2 Unique Cell Biology of Inflammation: Phagocytes

Polymorphonuclear neutrophils are the most abundant granulocytes circulating in the blood stream, and these cells are the first phagocytic cells responding to tissue insults and microbial infection. At this initial stage of inflammation, damage-associated molecular patterns (DAMPs) released by somatic cells attract neutrophils to the site [4]. One of the neutrophil's primary functions is to inactivate and kill invading microbes. The ability to phagocytose and eliminate invading microorganisms is critical for host defense. Neutrophils can ingest pathogens into phagosomes, which have an acidic, nutrient-deprived environment. In addition, phagosomes can fuse with special granules that contain proteases and antimicrobial peptides, and, more importantly, these specialized compartments can produce highly toxic levels of reactive oxygen species (ROS) for direct killing of pathogens (mostly bacteria) engulfed within. Besides this direct killing mechanism, neutrophils release proteases stored in their granules to modify the extracellular milieu or regulate other cell functions. In general, neutrophils are the first line of inflammatory phagocytes attracted to an injury site, where they perform their function and then undergo programmed cell death [5].

Circulating monocytes are another type of phagocyte that traffic via the blood stream to peripheral tissues in both homeostasis and inflammation. One unique feature of monocytes is their capability to differentiate into macrophages. When a monocyte enters a damaged tissue through the blood vessel, a process known as leukocyte chemotaxis and extravasation, it undergoes a series of changes to become a macrophage [6]. The maturation from monocyte to macrophage is triggered by local growth factors, such as pro-inflammatory cytokines and microbial products. Monocyte recruitment and maturation are critical for inflammation, and they contribute to effective control and clearance of bacterial, protozoal, fungal, and viral infections. It is worth noting that although there are stationary "resting" macrophages within healthy tissues, most macrophages that accumulate at diseased sites are functionally and biologically different and typically derived from circulating monocytes.

Once differentiated, mature and active macrophages can express cyclooxygenase-2 (COX-2) that produces prostaglandins [7]. Prostaglandins are locally acting, paracrine lipid mediators that promote vasodilation and inhibit the aggregation of blood platelets. Since prostaglandins are potent inflammatory triggers, specific COX-2 inhibitors have been developed for modulating inflammatory responses [8], although some show cardiotoxicity and significant safety concerns. Macrophages also express several other unique genes to facilitate their inflammatory functions. To cope with high-energy demand after maturation, macrophages express higher levels of folate receptor to increase folate uptake [9]. As the macrophages play an important role in tissue repair, they express several types of integrins on the plasma membrane to interact with the surrounding milieu and tissue scaffolds [10, 11]. In addition, macrophages can restructure tissue frameworks by secreting

many types of proteases specifically targeting components of the extracellular matrix (ECM) [12, 13].

Macrophages are also professional phagocytes, with an individual macrophage capable of digesting more than 100 bacteria during its life span. Similar to neutrophils, macrophages can ingest pathogens by engulfing them into phagosomes, which then fuse with lysosomes to form phagolysosomes. Intracellular phagolysosomes in macrophages contain enzymes and toxic reactive oxygen species (ROS) to digest and destroy their targets [14]. In addition to producing ROS in the intracellular compartments, activated macrophages can assemble ROS-producing machinery on the plasma membrane and release ROS into the nearby extracellular space. These ROS not only inactivate external targets directly but can also serve as chemical signals to coordinate with other cells [15]. However, unlike neutrophils which are short-lived and mostly die in the early stages of inflammation, macrophages survive longer in the body and are important regulators of inflammation at later stages. In addition to ingesting invading pathogens, macrophages are highly specialized in the removal of dying or dead cells and cellular debris. Thus, neutrophils and macrophages play their roles at different temporal stages of inflammation. In a typical bacterial infection scenario, neutrophils are attracted to the site of infection, where they perform their function, die, and are ultimately phagocytosed by the macrophages.

Compared to other somatic and stromal cells, phagocytes are specialized granulocytes with unique biochemical capabilities. They perform their inflammatory functions, either as effectors or regulators, by utilizing these unique enzymes or small mediator molecules. Given tissue inflammation is largely mediated by neutrophils and monocytes/macrophages, these cells and their biochemical armament could serve as possible targets for inflammation imaging. In the following sections, we will discuss how we can take advantage of these immune cell characteristics for noninvasively studying and quantifying inflammatory processes. In particular, the discussion will focus on phagocyte enzymes that are involved in ROS production and inflammatory proteases for zymogen activation.

1.3 Unique Inflammatory Enzymes for ROS Production

First, phagocytes have the capability to produce high levels of ROS. Activated phagocytes generate these highly reactive, oxygen-derived small molecules at sufficient levels to directly eliminate invading bacteria. However, at lower levels, ROS can also serve as signaling molecules to surrounding tissue. Superoxide ($O_2^{\cdot-}$) is the primary source of many downstream ROS, and in both neutrophils and macrophages, the phagocyte NADPH oxidase (Phox) is the major source of tightly controlled superoxide production [15]. Phox has multiple components/subunits and its activity can be regulated by its assembly. The major components include a membrane-bound heterodimer cytochrome b_{558} as the enzyme core, and several cytosolic regulatory subunits, including $p67^{phox}$, $p47^{phox}$, $p40^{phox}$, and Rac

[15]. Cytochrome b_{558} is a heterodimer protein consisting of subunit CYBA and CYBB. CYBB is a highly glycosylated transmembrane subunit of Phox (also known as $p91^{phox}$ and NOX2). More importantly, CYBB is the essential subunit which carries out the primary redox chain reaction from the cytosolic electron donor, NADPH, to the electron acceptor, oxygen, on the outside of the membrane [15]. Upon stimulation and activation, phagocytes assemble the complete Phox enzyme complex by recruiting cytosolic regulatory components (p67/p47/p40 and the GTPase Rac) to the membrane-bound cytochrome b_{558} core.

Interestingly, different phagocytes have different final assembly locations of Phox. At the initial stage of tissue damage and inflammation, neutrophils can consume high levels of oxygen to produce various ROS in the phagosome for their microbe-killing activities, a phenomenon called respiratory burst [16]. In resting neutrophils, most of the cytochrome b_{558} (CYBA/CYBB) is located in the membrane of intracellular storage granules, and only a small fraction is present in the plasma membrane [17]. Upon phagocytosis of opsonized bacteria, cytochrome b_{558} and all necessary regulatory subunits are transported to phagosomes where they are assembled into complete, active holoenzymes [15]. The enzyme complex is strategically placed on the granular membrane to release high levels of superoxide into the intragranular space of phagosomes. Of note, there are also several other enzymes in the phagosomes to further convert superoxide to various downstream ROS, greatly potentiating its toxicity toward microbes. For example, hydrogen peroxide (H_2O_2), another major ROS for killing bacteria, can be generated by spontaneous dismutation of superoxide particularly at low pH within phagosomes. Alternatively, but to a lesser extent, hydrogen peroxide production can be facilitated by superoxide dismutase (SOD) [15]. Hydrogen peroxide can be further converted to other downstream antimicrobial ROS such as hypochlorous acid (HOCl) in the presence of myeloperoxidase (MPO) [18]. Thus, the respiratory burst is a phenomenon of neutrophils using phagosomal enzymes such as Phox and MPO to rapidly convert high levels of oxygen into a variety of toxic ROS.

On the other hand, macrophages are known to produce extracellular ROS, but at a lower level. When macrophages emerge as secondary responders at sites of inflammation, they play various regulatory roles and small, reactive ROS serve as signaling molecules. One of the primary functions of macrophages is to coordinate with other cell types to achieve tissue repair. The ROS generated by macrophages at later stages of inflammation have multiple regulatory functions, including tissue remodeling, new vessel formation, and reepithelialization [19]. Therefore, unlike in neutrophils, cytochrome b_{558} in macrophages is mostly found in the plasma membrane with low levels present in the intracellular compartments [20], to serve as a recycling pool of the enzyme core [21]. Furthermore, macrophages show low levels of MPO expression in intracellular vesicles that are not sufficient for high-level hypochlorous acid production as seen in neutrophils [22]. Thus, neutrophils use Phox to produce high levels of internal ROS for direct microbe killing, while macrophages use Phox to generate lower levels of external superoxide predominantly for regulatory functions [20].

1.4 Unique Inflammatory Proteases

In addition to ROS-related enzymes, phagocytes produce and/or secrete various proteases to facilitate their antimicrobial, tissue remodeling, and other inflammatory functions. For example, neutrophil elastase is a serine proteinase stored within specialized neutrophil lysosomes, called azurophil granules. When released from activated neutrophils, neutrophil elastase has a direct antimicrobial function. It is known to degrade the outer membrane protein A (OmpA) of *E. coli* as well as other virulence bacterial factors found in *Shigella*, *Salmonella*, and *Yersinia* [23]. In addition to elastin, neutrophil elastase has a broad substrate range beyond what its name suggests. The enzyme can hydrolyze other protein components of the extracellular matrix, including aggrecan, fibronectin, the triple-helix structure of type III and IV collagens, and the cross-linkage regions of type I, II, and V collagens [24]. It has been shown that neutrophil elastase is present in considerable concentrations outside of the neutrophil at sites of chronic inflammation, and its serine proteinase activity has been linked to the pathologic processes of a variety of inflammatory diseases, including idiopathic pulmonary fibrosis, rheumatoid arthritis, adult respiratory distress syndrome, and cystic fibrosis. Released neutrophil elastase may regulate inflammation by digesting and processing various inflammation-promoting factors in the extracellular matrix, an idea supported by recent studies showing the involvement of neutrophil elastase in degenerative and inflammatory disorders [25].

Matrix metalloproteinases (MMPs) are another class of protease commonly associated with tissue inflammation. MMPs are zinc-dependent endopeptidases produced by many cell types, including lymphocytes and granulocytes, but in particular by activated macrophages [13]. Macrophages secrete a broad range of MMPs, and these specialized phagocytes represent a major source of MMPs in chronic inflammatory lesions such as granulomas [26]. Like many proteases with potent regulatory functions, MMP activities are carefully controlled. They are initially synthesized as inactive proenzymes (zymogens) with a pro-peptide domain that must be removed before the enzyme is active. For example, pro-MMPs can be activated by neutrophil elastase [27]. MMPs are capable of degrading a wide range of extracellular matrix proteins, and thus they play important roles in various physiological and pathological processes involving tissue remodeling. MMP activities are associated with morphogenesis, angiogenesis, tissue repair, cirrhosis, arthritis, and metastasis. More interestingly, the roles of MMPs are not only limited to tissue remodeling, as they also modulate the immune response by cleaving cytokines and chemokines to control leukocyte migration. In turn, cytokines and chemokines activated and released by MMPs can control surrounding cell behavior such as cell proliferation, migration (adhesion/dispersion), differentiation, angiogenesis, apoptosis, and host defense [28]. They can also control cell death by specific cleavage of cell surface receptors and the release of apoptotic ligands (such as the Fas ligand). Therefore, it is not surprising that MMPs have been found to be involved in many human diseases. Studies indicate that MMP-2 and MMP-9 are particularly important in cancer metastasis [29], while MMP-1 is thought to be important in rheumatoid arthritis and osteoarthritis [30].

Cathepsins (Cat) belong to a family of proteases commonly found in all animals as well as most other organisms, and some of them are implicated in inflammatory responses. There are approximately a dozen members of this family, and they are categorized by their structure, catalytic mechanism, and which proteins they cleave [31]. Currently, the cathepsin family includes two serine proteases (Cat A, Cat G), two aspartic proteases (Cat D, Cat E), and 11 lysosomal cysteine proteases (Cat B, C, F, H, K, L, O, S, V, X, and W). Like many proteases, cathepsins are initially synthesized as inactive proenzymes that need to be proteolytically processed for activation [32]. Many cathepsins become activated at the low pH found in lysosomes, and as a result, most Cat activities are observed intracellularly and, in particular, within these organelles. However, there are secretory cathepsins that operate extracellularly. One of the important examples is Cat K, a cysteine protease that is known to be secreted into the extracellular space by osteoclasts to facilitate bone resorption. Furthermore, macrophages secrete Cat K in inflamed tissues, and so can some fibroblasts and epithelial cells, albeit to a lesser degree [12]. Monocyte-derived macrophages express and secrete Cat K after 6 or 12 days of differentiation [12, 33]. In addition, a variety of cysteine cathepsins are key regulatory proteases in inflammation [34]. Cat B, C, F, H, and L are also known to be expressed by macrophages. In macrophages and microglia, cysteine Cat S is initially present within the cells; however, upon phagocyte activation, Cat S activity is released extracellularly [35]. Furthermore, antigen-presenting cells (APCs), including dendritic cells (DCs) and B lymphocytes, are known to express Cat S [36].

1.5 Advantages of Whole-Body Optical Imaging for Inflammation Research

In inflamed tissue, many biochemical, physiological, and pathological processes occur, as does communication or crosstalk between many cellular players, making it rather difficult to reproduce such environments in vitro. Furthermore, inflammation is not a simple, static phenomenon that can be characterized by a simple endpoint measurement. It is a dynamic process evolving with time as different immune cells enter, exit, and/or die at inflammatory sites. Thus, it is necessary to use living animal models for inflammation research, with research tools that can capture the dynamic nature of inflammation. However, using animals for research presents several challenges, including the acquisition of repeated measurements of the animal model in a longitudinal observation. Traditionally, histological techniques are the gold standard for detecting the presence of inflammatory phagocytes in tissues. However, as tissue collection typically requires animal termination, histological approaches are not capable of following inflammation processes in the same animals over time. In addition, histological methods generally require much higher number of animals in a cohort, which is especially true when engaging in a longitudinal study involving many sample-collecting timepoints. Therefore, histological methods are

questionable from an animal welfare point of view and also too costly for longitudinal studies, and they are typically used only for endpoint assessment.

In this regard, noninvasive molecular imaging techniques have several advantages that can greatly help researchers to better understand the inflammatory processes in living subjects. Currently, there are several imaging methods available for imaging inflammation in living animals. These methods include optical imaging (chemiluminescence or fluorescence, in the visible and near-infrared range), positron emission tomography (PET), single-photon emission computed tomography (SPECT), magnetic resonance imaging (MRI), X-ray-based computed tomography (CT), and ultrasound (US). Each method has its strengths and can be used to visualize certain, but not all, aspects of tissue inflammation in living animals. Nevertheless, the noninvasive nature of these technologies makes it possible to combine more than one of these imaging modalities into an animal study for a more comprehensive view of disease progression.

Optical imaging has several advantages over the nonoptical imaging methods. Unlike PET or SPECT that detect high-energy, short-wavelength radiation emitted from unstable radioactive isotopes, optical methods use stable, safe, and nonradioactive probes that produce light signals in the visible, far-red, or near-infrared (NIR) range (400–800 nm) of the electromagnetic spectrum. This means that optical imaging does not require dedicated space and special shielding for safety; therefore, optical imaging instruments are much less regulated and are more accessible for researchers (with less shielding needed for fluorescence excitation lasers). In vivo optical imaging instruments are generally less expensive than PET, SPECT, and MRI imagers, and most optical imaging probes generally are less expensive than radioactive tracers. Thus, optical modalities have lower operational expenses and are more easily accessible for researchers. In addition, optical imaging can provide quantitative assessment of biological changes. Although MRI, CT, and US are highly useful modalities for anatomical and functional visualization, it is not easy to use them for quantitative assessment of unique inflammatory cells or biological processes, even with the help of contrast-modulating agents. On the other hand, optical imaging data can be easily quantified since inflammatory target signals can be calculated in terms of photoemission from the inflamed tissues, and in tomographic optical imaging, it is also possible to quantify the amount of localized probes in terms of molar concentrations or total nanomoles or picomoles. The scope of this review will focus on the strengths of optical imaging methods and discuss imaging strategies that take advantage of unique and specific inflammatory ROS enzymes and proteases for imaging inflammation in living animals.

Of note, since optical imaging operates in the visible and NIR spectral range (400–800 nm), the scattering of light limits its spatial resolution to slightly below a millimeter [37]. Further, as visible light in the 400–600 nm range can be significantly attenuated by hemoglobin, optical imaging methods operating in the visible light spectrum have detection depth typically less than 10 mm. Fortunately, the tissue penetration of optical signals can be greatly improved by using NIR light sources (700–800 nm or above) and fluorescent probes. The use of fluorescent probes has

another advantage over the radioactive tracers, as their distribution in the target tissues can be further validated by fluorescence microscopy.

1.6 Chemiluminescence Imaging (CLI) and Fluorescence Imaging (FLI): An Overview

In vivo optical imaging techniques can be generally categorized by the mode of light excitation: chemiluminescence imaging (CLI) or fluorescence imaging (FLI). The main difference between CLI and FLI is the energy source for photon generation. CLI uses chemical compounds as the energy source [38], whereas FLI utilizes excitatory light as the energy source. As external excitatory light sources have much higher-energy output, FLI typically requires shorter exposure time and less pixel binning during image acquisition. On the other hand, since CLI uses injected chemical compounds as the energy sources, the CLI light signals are much dimmer in comparison. Therefore, to improve imaging sensitivity, CLI generally requires longer exposure and larger binning which makes the images more pixelated in presentation.

FLI can measure a broad variety of physiological endpoints with a variety of biologically targeted or enzyme-activatable fluorescent probes. Nevertheless, the use of FLI in living animals can be limited by tissue auto-photoluminescence at certain wavelengths due to the inherent short Stokes shifts (~20–40 nm) of most dyes [39]. CLI has certain advantages over FLI. Without the need for excitation light, CLI has lower background signal and thus can often yield higher signal-to-noise (S/N) ratios and better sensitivity. Bioluminescence imaging (BLI) is a unique type of CLI imaging that utilizes specific enzyme-substrate pairs (e.g., luciferase-luciferin) to further improve signal strength and specificity [40, 41]. However, the potential of BLI for in vivo application in inflammation imaging is limited due to the need for ectopic expression of luciferase in the inflamed tissues and restricted by a rather small selection of compatible luciferase-luciferin pairs [42, 43]. Thus, this review will focus mostly on CLI imaging for inflammation using chemical compounds.

2 Imaging Inflammation Using ROS-Sensitive Chemiluminescent Compounds

2.1 Small Chemiluminescent Compounds

Since inflammation is a multistep in vivo process involving a variety of specialized inflammatory cells and enzymes, molecular imaging methods specifically targeting these unique features would allow noninvasive, accurate assessment of inflammation

status in a longitudinal manner. The CLI strategies for inflammation imaging mainly take advantage of the unique ROS enzymes in inflammatory phagocytes. These enzymes can produce superoxide and its downstream reactive oxygen species that can react with CLI compounds. Many small chemiluminescent compounds have been widely used in laboratories as chemical assays to detect different types of ROS. One of the most important examples is luminol ($C_8H_7N_3O_2$, MW = 177.2). Luminol can react with hydrogen peroxide (H_2O_2) to generate blue chemiluminescence. However, the luminol-based chemiluminescence reaction requires the presence of a catalyst such as a peroxidase to promote light production. Other small CLI probes such as lucigenin ($C_{28}H_{22}N_4O_6$, bis-N-methylacridinium nitrate, MW = 510.5) [44] and methylated *Cypridina* luciferin analogs ($C_{14}H_{14}ClN_3O_2$, MCLA hydrochloride, MW = 291.7) are commonly used in laboratories as well. They are specific chemiluminescence compounds for the detection of superoxide anions (O_2^-) and singlet oxygen ($^1O_2$) in vitro and ex vivo [45]. However, unlike luminol, lucigenin and MCLA can react with ROS and produce chemiluminescence without the presence of a peroxidase. In addition, it is worth noting that these small chemiluminescent compounds, luminol, lucigenin, and *Cypridina* luciferin analogs, all produce light in the blue region of visible light at around 450 nm, which has limited tissue penetration due to strong absorbance by heme in this spectral region. Figure 1 summarizes these small CLI compounds (luminol, lucigenin, and MCLA) and their reaction requirements for light production.

Despite the extensive use of small CLI compounds for in vitro assays, their potential for in vivo imaging of superficial sites of inflammation was only recently examined. With their specific affinity for ROS, these chemiluminescence compounds were tested for in vivo inflammation imaging and found to react with inflammatory ROS to generate inflammation-specific chemiluminescence in living animals. More importantly, they demonstrated acceptable pharmacological properties and were generally well tolerated when injected into mice. Luminol and its derivative L-012 ($C_{13}H_8ClN_4O_2$, sodium salt) are capable of generating blue chemiluminescence in several animal models of inflammation [46–48]. Lucigenin can also produce chemiluminescent signal; however, further investigation indicates luminol and lucigenin target different inflammatory phagocytes and have different light-producing mechanisms in the used animal models. Interestingly, it has been shown that luminol bioluminescence in vivo is mediated by neutrophils, while lucigenin bioluminescence is mediated by macrophages [49]. Such a difference makes it possible to use luminol and lucigenin imaging to distinguish early and late phases of inflammation [49]. Since these small compounds are commercially available and relatively inexpensive, they can be readily translated to many inflammation imaging applications in small animals. Figure 2 illustrates the difference in phagocyte imaging mechanisms of these two small CLI compounds. This pair of compounds allows differential visualization of neutrophils and macrophages in a noninvasive manner, thus allowing the longitudinal assessment of these cell populations both in the acute and chronic phases of inflammation.

Two factors determine the different specificities of these two compounds toward phagocytes. The first factor is the difference in membrane permeability. Luminol

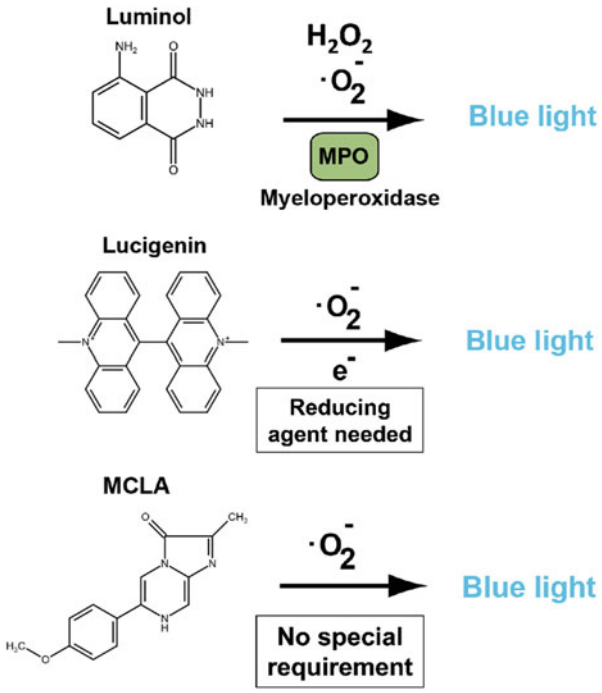

Fig. 1 Mechanism of small chemiluminescence probes for ROS detection and imaging in living animals. Luminol, lucigenin, and the methylated *Cypridina* luciferin analog (MCLA) are small CLI probes capable of producing blue chemiluminescence in response to ROS. Luminol reacts with superoxide or hydrogen peroxide (H_2O_2). However, luminol chemiluminescence requires a catalyst such as a peroxidase to promote light production. In living animals, myeloperoxidase (MPO) is responsible for this catalytic role. Other small CLI compounds such as lucigenin and the methylated *Cypridina* luciferin analog (MCLA hydrochloride) can react with the superoxide anion ($\cdot O_2^-$) and singlet oxygen ($^1O_2$) without any peroxidase. However, lucigenin chemiluminescence requires a reducing agent for its activation. In biological systems, NADH or NADPH are the typical reducing agents for lucigenin activation

(MW = 177.2) is a small uncharged molecule that can easily penetrate both the plasma membrane and the membrane of intracellular vesicles (such as phagosomes). On the other hand, lucigenin is a larger molecule (MW = 510.5) with two positive charges, making it much less membrane-permeable. The second and more critical factor is the difference in subcellular locations in neutrophils and macrophages where the Phox holoenzyme assembles.

Although both luminol and lucigenin depend on Phox to provide superoxide anion ($O_2\cdot^-$), in living subjects, luminol bioluminescence also relies on peroxidase activity to catalyze the light-emitting reaction [46, 49]. Prior studies have indicated that myeloperoxidase (MPO) is the peroxidase responsible for luminol luminescence in vivo. In neutrophils (or monocytes), high levels of MPO are found in the intracellular vesicles (phagosomes), where most of the Phox is present [18]. As a result, luminol bioluminescence is preferentially generated within phagosomes of activated neutrophils (or monocytes, to a lesser extent). Interestingly, as acute

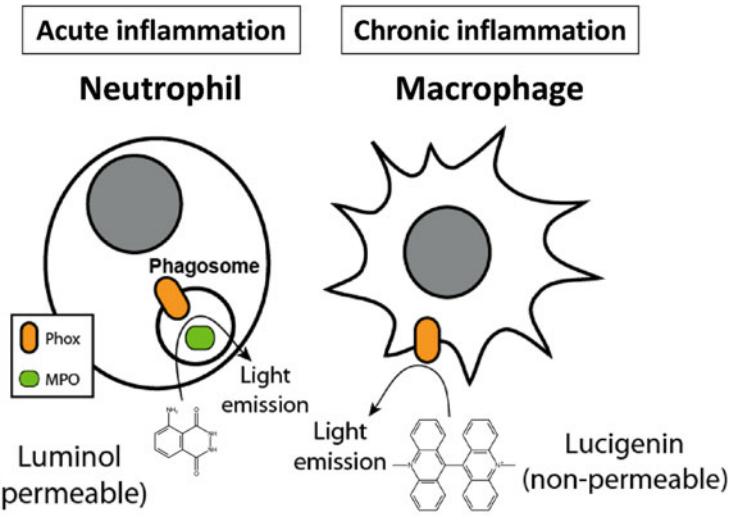

Fig. 2 Phagocyte NADPH oxidase (Phox) is the major source of superoxide produced in inflammatory phagocytes. Phagocyte NADPH oxidase has multiple components and is responsible for the CLI luminescence observed in living animals. Upon activation, granulocytes such as neutrophils assemble Phox in the membrane of intracellular storage granules. Neutrophils (granulocytes) also express high levels of myeloperoxidase (MPO) in the granules. In contrast, activated macrophages assemble Phox in the plasma membrane after activation. The difference in subcellular locations of Phox holoenzyme assembly enables the use of luminol and lucigenin to image specific phagocyte populations. Luminol is a small uncharged molecule that can easily penetrate both plasma membrane and membrane of intracellular vesicles in the neutrophils, where MPO is also present. On the other hand, lucigenin is a larger molecule with two positive charges, making it much less membrane-permeable and therefore it can be used for imaging plasma membrane-bound Phox activity in macrophages

inflammation is mostly mediated by neutrophils, the fact that MPO activity is predominantly present in neutrophils makes luminol ideal for imaging early inflammatory responses. Therefore, luminol is not suitable for monitoring late-phase or chronic inflammation, in which neutrophils are believed to play a lesser role in comparison to macrophages.

On the other hand, lucigenin is more specific for imaging macrophage activity in animal inflammation models [49]. After maturation from circulating monocytes, macrophages in the tissue tend to lose most of their MPO activity [22], and thus cannot be effectively visualized using luminol. Lucigenin can react with extracellular ROS produced by macrophages in chronically inflamed tissues to produce chemiluminescence. Unlike neutrophils, whose Phox activities are mostly in the intracellular granules, macrophages assemble Phox in the plasma membrane after activation [20]. Therefore, the membrane-impermeable lucigenin selectively interacts with superoxide produced by macrophage Phox in the extracellular space and produces CLI signals indicative of late-stage inflammation.

Figure 3 demonstrates the use of these two CLI compounds to distinguish between early and late stages in a murine skin inflammation model. Local and

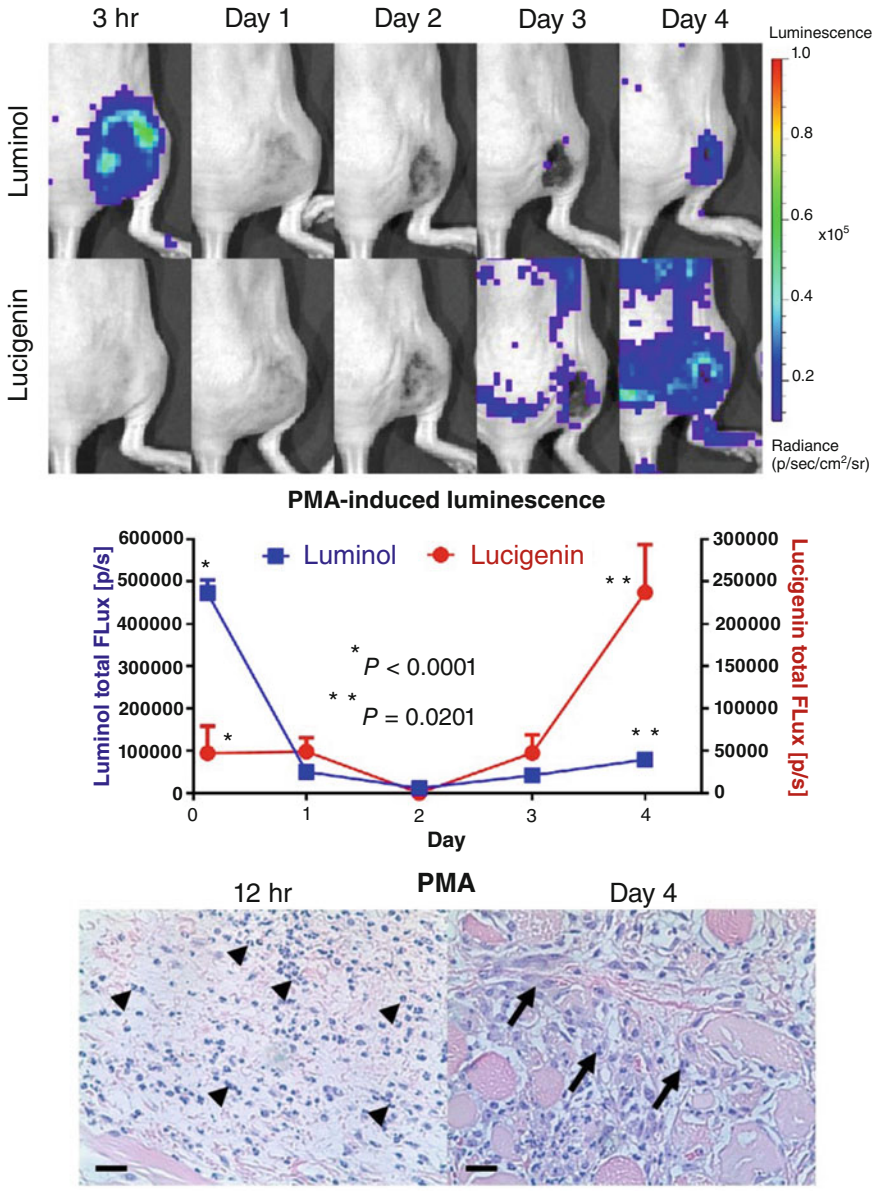

Fig. 3 Luminol and lucigenin image different stages of inflammation responses. Subcutaneous injection of phorbol 12-myristate 13-acetate (PMA) causes rapid skin irritation and inflammation. Daily imaging (top) of both lucigenin and luminol bioluminescence was performed for 4 days. Using an IVIS® Spectrum imaging system, significant luminol chemiluminescence from the injection sites were observed as early as 3 h after PMA injection, while very low lucigenin luminescence was observed. However, from day 3 onward, as wound contraction and scar formation were visible, a steady increase of lucigenin bioluminescence was observed (middle graph). These results suggest that luminol bioluminescence is associated with the acute phase of

superficial inflammation can be induced by subcutaneous injection of phorbol 12-myristate 13-acetate (PMA), a potent protein kinase C (PKC) activator capable of causing rapid skin irritation and inflammation. The preferential affinity of luminol for neutrophils makes it ideal for visualizing acute inflammation, whereas very low lucigenin luminescence is observed at this early stage. However, as macrophages move into the inflamed skin tissue to orchestrate wound repair and scar formation, lucigenin luminescence prevails at this later inflammatory stage. Further mechanistical studies using *Cybb* or *Mpo* knockout mice have demonstrated the different chemiluminescence mechanisms of these two CLI compounds. Although both luminol and lucigenin need Phox as the superoxide source, lucigenin does not require a peroxidase such as MPO to produce light (Fig. 4). The chemiluminescence reaction of lucigenin involves two key steps [50]. The first step is single-electron reduction of lucigenin (LC^{++}) to form lucigenin cation radical ($LC^{\cdot+}$). The second step is for the radical intermediate to react with superoxide anion ($O_2^{\cdot-}$) to produce light. Superoxide by itself is not able to reduce lucigenin. It has been demonstrated that an additional reducing agent, such as NADH or NADPH, is required for ex vivo measurement of superoxide anion level in tissue homogenates [51]. In living tissues, plasma membrane-bound Phox in macrophages can facilitate both steps by single-electron reduction of extracellular lucigenin using intracellular NADPH as an electron donor and provide superoxide to complete the chemiluminescent reaction, making it ideal for imaging macrophages (Fig. 4). One concern regarding the use of lucigenin for CLI is its possible redox cycling, a phenomenon that typically occurs when lucigenin is used to measure ROS in vitro or ex vivo. In this alternative mechanism, the lucigenin cation radical ($LC^{\cdot+}$) intermediate, instead of reacting with superoxide to produce light, may reduce oxygen (O_2) to produce artificial superoxide ($O_2^{\cdot-}$) [47]. However, redox cycling is not likely to happen in live animals since living tissues have rather low oxygen pressure (~10 mmHg, compared with ~150 mmHg in the atmosphere). In living tissues, the positively charged radicals would have much higher affinity for endogenous superoxide anion ($O_2^{\cdot-}$, with a negative charge opposite to $LC^{\cdot+}$) than for the uncharged oxygen (O_2) [51]. The fact that macrophage Phox generates both lucigenin cation radical ($LC^{\cdot+}$) and superoxide anion ($O_2^{\cdot-}$) in the vicinity of extracellular space greatly facilitates lucigenin chemiluminescence and therefore makes lucigenin a selective CLI compound for macrophage imaging.

Fig. 3 (continued) inflammation, whereas lucigenin bioluminescence is preferentially associated with the late phases of inflammation. Skin samples collected at 12 h and 4 days after PMA injection show different phagocyte presence (bottom rom) in the inflamed tissue according to H&E staining (scale bar: 20 μm). At the early stage (12 h), granulocytes, mostly neutrophils, are the predominate phagocytes. On the other hand, macrophages are the dominant type at a late inflammation stage (day 4). Images shown are original data from a related published study [49]

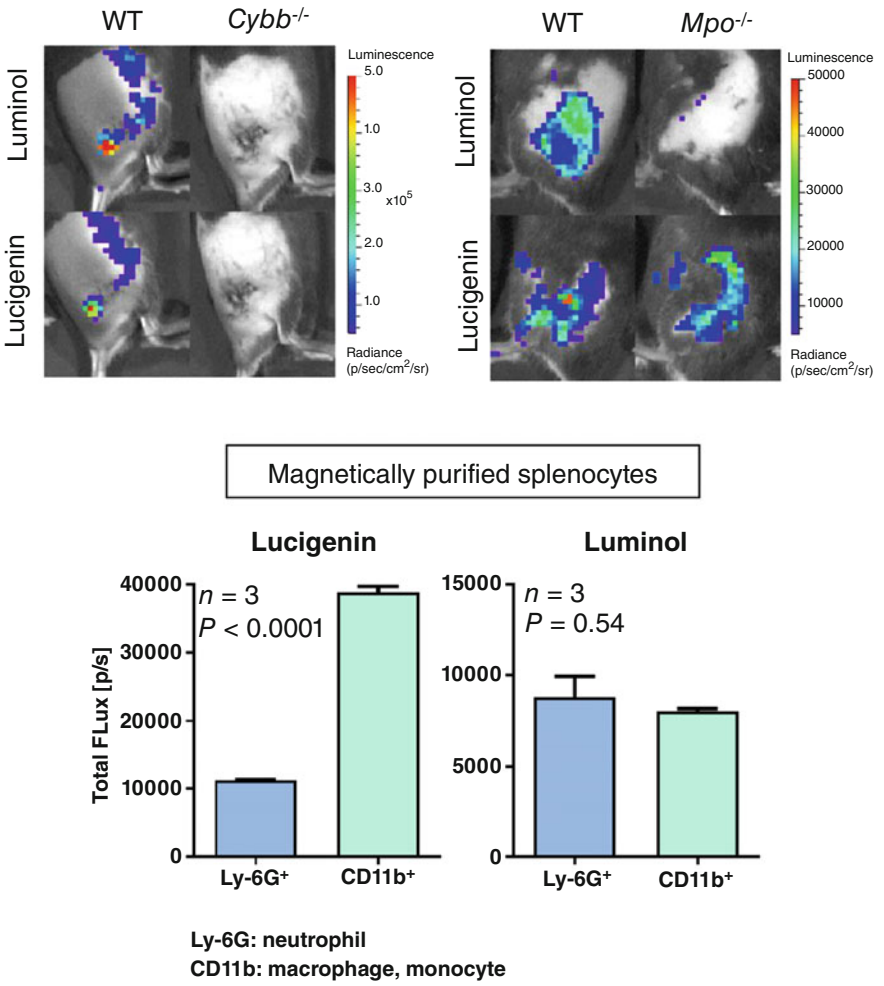

Fig. 4 Mechanistic studies of luminol and lucigenin chemiluminescence using knockout mice. Inflammatory CLI was performed in *Cybb*$^{-/-}$ and *Mpo*$^{-/-}$ mice to examine the roles of Phox and MPO in chemiluminescence produced by lucigenin and luminol. CYBB is the key component of Phox holoenzyme. *Top row*: in one study, surgical skin wounds were made in both WT and *Cybb*$^{-/-}$ mice and imaging of both CLI compounds was performed 4 days later. Using an IVIS® Spectrum imaging system, very low CLI signals of both lucigenin and luminol were observed in *Cybb*$^{-/-}$ animals, indicating that Phox is necessary for both lucigenin and luminol bioluminescence. In another set of studies, local tissue inflammation was induced by subcutaneous (s.c.) injection of PMA into wild-type (WT) and *Mpo*$^{-/-}$ mice. Acute-phase luminol luminescence signals were acquired 3 h after PMA injection, and late-stage lucigenin chemiluminescence was visualized 3 days after PMA injection. MPO deficiency greatly affected luminol bioluminescence, especially in the early phase of inflammation, while lucigenin bioluminescence did not depend upon MPO activity. *Bottom row*: magnetically purified Ly-6G$^+$ neutrophils and CD11b$^+$ macrophages/monocytes were stimulated with PMA in vitro. The CD11b$^+$ cells produced higher lucigenin bioluminescence than Ly-6G$^+$ cells, indicating that macrophages and/or monocytes preferentially activate lucigenin. In contrast, luminol bioluminescence showed no significant difference between

2.2 *Energy Transfer Luminescence Imaging Using Small CLI Substrates as Energy Sources*

Small CLI compounds in general have good signal-to-noise ratios (S/N) for visualizing inflammatory processes in living animals. However, an immediate drawback of using these small CLI compounds for animal imaging is that their light emissions are mostly in the blue range (~450 nm). Several strategies have been pursued to make them emit light of longer wavelengths to improve tissue penetration. The general concept is to use small CLI compounds as the energy sources, and upon reacting with ROS, the chemical energy is transferred to a nearby acceptor fluorophore to generate red-shifted light emission [52]. There are two types of energy transfer strategies: chemiluminescence *r*esonance *e*nergy *t*ransfer (CRET) and chemically initiated electron-exchange luminescence (CIEEL). Both energy transfer strategies attempt to address the blue color issue by combining the strength of both chemiluminescence and fluorescence imaging. CIEEL, like CRET, also uses chemical energy stored within CLI compounds to generate proximity-dependent luminescence. Nevertheless, these two techniques are fundamentally different in their energy transfer mechanisms and therefore have different application scenarios.

CRET has a Förster (resonance) energy transfer mechanism as used in fluorescence resonance energy transfer (FRET). The Förster resonance energy transfer mechanism is based on dipole-dipole coupling and thus requires spectral overlap between the energy donor's emission and the recipient's absorbance spectra for efficient energy transfer and subsequent light emission. Therefore, the recipient is typically a fluorescent dye whose excitation wavelength matches well with the donor CLI compound's emission wavelength, but capable of emitting red-shifted light. In theory, the operational distance for Förster energy transfer is 10–100 Å [53], and therefore CRET can be used to visualize larger molecule interaction such as protein-to-protein or protein-to-nucleic acid in vitro. Several ROS-sensing small microbeads or nanoparticles have been developed and are commonly used for in vitro binding assays and applications [54]. For in vivo CRET applications, luminol-based ROS imaging strategies have been used to visualize inflammation in deep tissues [55]. In addition, as luminol emits blue chemiluminescence upon activation, it is suitable for pairing with NIR quantum dots or nanoparticles (conjugated or in free form) that efficiently absorb blue light for imaging deep tissue inflammation [55].

Figure 5 illustrates a CRET imaging strategy to visualize phagocyte ROS production using microbeads specifically designed for amplified luminescence proximity homogeneous assay (ALPHA) technology. These ALPHA acceptor beads can

Fig. 4 (continued) Ly-6G$^+$ and CD11b$^+$ cells, suggesting that MPO was present in both cell types. Together, these results suggest that lucigenin bioluminescence is not mediated by neutrophils, as is the case for luminol. Images shown are original data from a related published study [49]

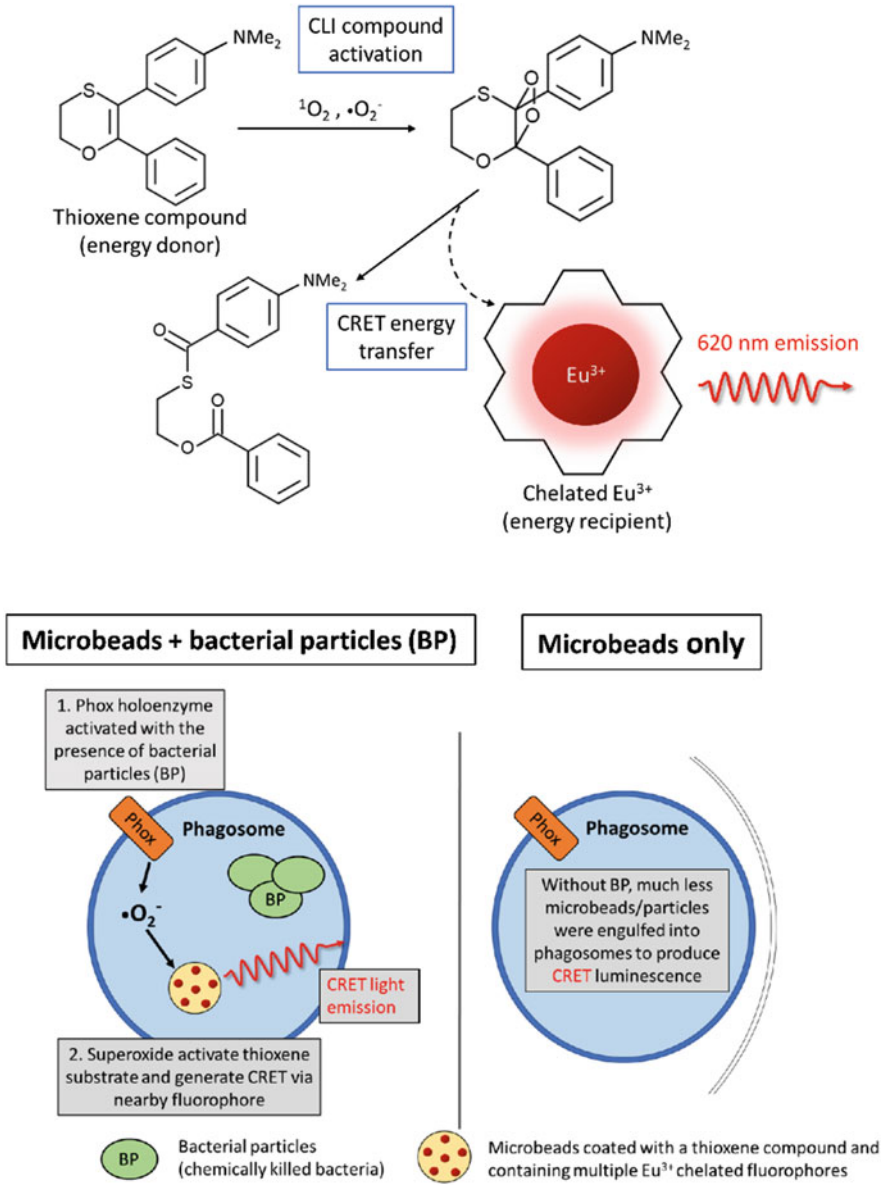

Fig. 5 Thioxene/europium microbeads produce CRET luminescence in response to ROS produced by phagocytes. The amplified luminescence proximity homogeneous assay (ALPHA) acceptor microbeads are coated with thioxene compounds that serve as the energy donor. *Top row*: the thioxene compound can react with singlet oxygen or superoxide anion to form a high-energy intermediate. To ensure efficient energy transfer and CRET light production, the bead is embedded with several europium (III) chelate complexes acting as energy recipients that emit red CRET light at ~620 nm. *Bottom row*: to image inflammatory ROS produced by phagocytes, the microbeads can be mixed with chemically killed *Staphylococcus aureus* bacterial particles (BP) to trigger efficient

produce luminescence in response to ROS such as the superoxide anion and singlet oxygen [54]. The microbeads are about 250 nm in diameter and have a chemiluminescent thioxene coating that serves as the CLI energy source to react with ROS. In addition, embedded within the beads are multiple europium (III) chelate complexes that serve as CRET energy recipients. In this configuration, energy transfer between the ROS-activated small CLI chemical compound (thioxene) and the energy recipient (chelated Eu^{3+}) is ensured. In living animals, locally injected ROS-sensing microbeads can detect ROS produced downstream of Phox in phagocytes. Figure 6 demonstrates the use of these beads to visualize red CRET light signals produced by inflammatory phagocytes. However, their application in in vivo imaging is rather limited, mostly due to the larger size of the microbeads or nanoparticles in comparison to small CLI substrates. The large size of microparticles make them less ideal for systemic delivery, and therefore they are mostly used for imaging local inflammation, for example, in bacterial infection models [56].

Similar footpad inflammation studies were performed on WT and *Cybb*$^{-/-}$ mice. As CYBB is the critical catalytic subunit for Phox function, mice lacking CYBB cannot produce high levels of superoxide in the phagosomes, and very little CRET light signals were observed in the *Cybb*$^{-/-}$ footpads inoculated with both ALPHA microbeads and BPs. These results indicate phagosome Phox is responsible for the Alpha microbead CRET light signals in this inflammation model.

Other Förster energy transfer strategies, such as bioluminescence resonance energy transfer (BRET), also use chemical energy stored within luciferins to generate proximity-dependent luminescence. The major difference between CRET and BRET is how the small high-energy chemical molecules (either CLI compounds or luciferins) are activated. CRET relies on ROS to trigger CLI substrate activation, while BRET requires specific luciferase enzymes to release the energy stored within luciferins. Since BRET is also based on the Förster energy transfer mechanism, it has similar operational distance (10–100 Å) and spectral requirement between the energy donor (in this case, a luciferin) and the recipient. Thus, it is also possible to use BRET to visualize interactions between larger molecules. In laboratories, BRET has been adapted for microscopic imaging of protein-protein interactions in living cells using luciferase/photoluminescent protein pairs such as *Renilla* luciferase/YFP. However, in vivo applications of BRET for whole-animal imaging have been hindered by the need for exogenous introduction of chimeric target proteins, and by tissue attenuation of blue-green light signal [57, 58]. To improve tissue penetration, *Renilla* luciferase has been conjugated with quantum dots and polymer

Fig. 5 (continued) uptake of both the microbeads and BPs into the phagosome (lower left). Once inside the phagosome, superoxide produced by Phox can activate the thioxene compound and transfer its energy to the embedded fluorescent recipients for CRET light emission. In the absence of BP (lower right), fewer microbeads are engulfed into phagosomes and only very low CRET signals are detected

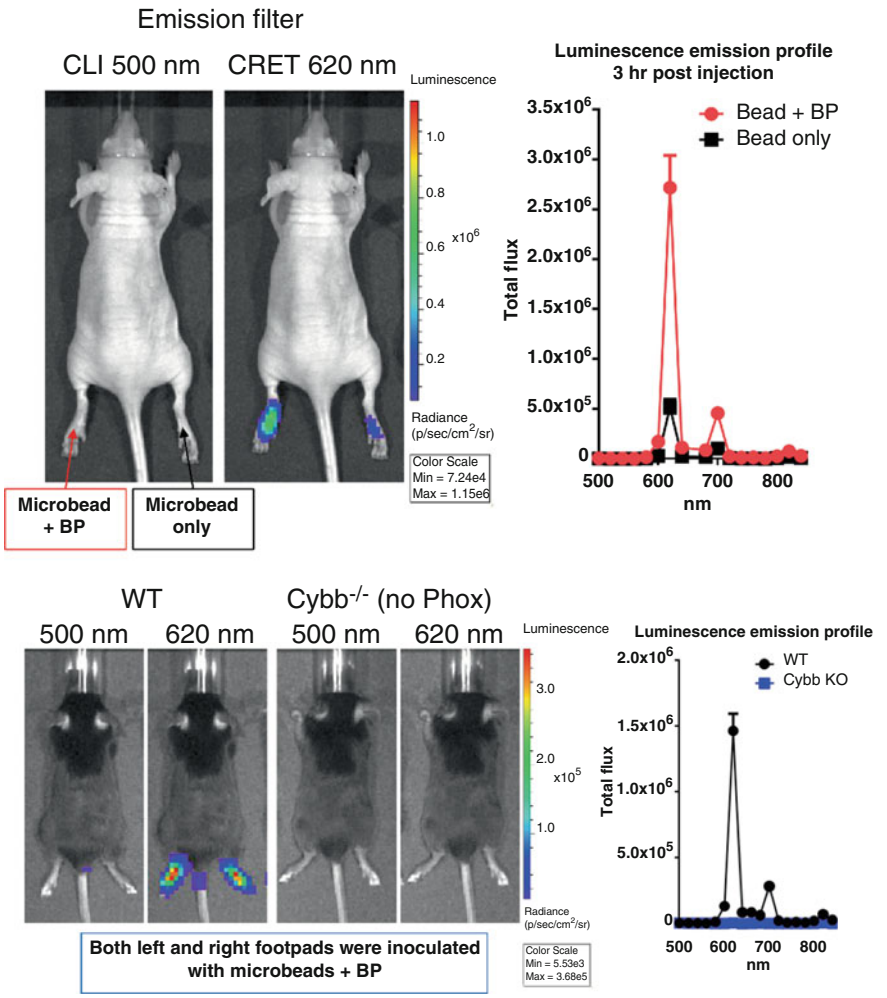

Fig. 6 In vivo CRET energy transfer imaging using ROS-sensitive thioxene/europium microbeads. In this example, ALPHA acceptor microbeads were mixed with chemically killed *Staphylococcus aureus* bacterial particles (BP) prior to subcutaneous injection into the left hind footpad. The bacterial component ensures efficient uptake of both the BP and microbeads (left hind footpad). Once inside the phagosome, superoxide produced by Phox can activate the microbeads to produce CRET light emission which can be readily visualized using the IVIS® Spectrum imaging system. In the absence of BP (right hind footpad), fewer microbeads were engulfed into phagosomes and only low CRET signals were observed. Interestingly, spectral analysis of the emitted luminescence showed red light of 620 nm wavelength which was the major light emission without significant blue light emission, indicating efficient CRET energy transfer of ALPHA microbeads in this footpad inflammation model. Images shown are original data from an unpublished study

nanoparticles to generate far-red or NIR BRET luminescence [59, 60]. These limitations make BRET a more challenging approach for in vivo inflammation imaging.

Another energy transfer strategy for inflammation imaging is based on chemically initiated electron-exchange luminescence (CIEEL). Unlike Förster energy transfer, CIEEL energy transfer mechanism does not require spectral overlap between the energy donor (e.g., small chemical compounds, luciferin) and the fluorescent recipient. Instead, CIEEL has a charge-exchange mechanism that requires wave function overlap for direct intermolecular electron transfer between the donor and the recipient. Therefore, CIEEL operates in a much shorter length scale (<10 Å) than CRET/BRET. In other words, the CIEEL energy transfer is initiated by direct intermolecular collision between the chemical energy donor and the fluorescent recipient molecules [61–63]. If such short-range interaction can be achieved, CIEEL has an appealing advantage over CRET: CIEEL does not require spectral overlap between the energy donor and the recipient. Although CIEEL is not governed by spectral compatibility, efficient energy transfer is largely determined by the accessibility of the donor and the recipient for intermolecular collision. Therefore, CIEEL energy transfer imaging could take advantage of a broader repertoire of fluorescent probes for customizable biological readouts. It is also possible to use the same small compound as the energy source to drive a variety of fluorescent recipients for CIEEL luminescence at different colors.

The best studied example of CIEEL is the glow stick. Commercially available glow sticks utilize peroxyoxalates, such as bis-2,4,6-(trichlorophenyl)-oxalate (TCPO), as the chemical energy source. Figure 7 illustrates the general CIEEL mechanisms using small chemical compounds as energy sources. After snapping a glow stick, TCPO in the inner tube reacts with hydrogen peroxide in the outer tube to produce 1,2-dioxetanedione, a high-energy intermediate [61, 62]. In the absence of any energy recipient, the high-energy intermediate fragments into two molecules of carbon dioxide and releases its chemical energy as UV emission or heat dissipation. However, in the presence of a fluorescent recipient in the near vicinity, the chemical energy can be transferred via formation of a charge-transfer complex of the intermediate and the fluorescent recipient [63]. Thus, glow stick luminescence is fundamentally different from Förster-based CRET or FRET [53, 64]. Using the same chemical substrate TCPO as the energy source, it is possible to manufacture glow sticks in a wide range of colors as the color is solely determined by the fluorescent recipient added into the tubes.

Since CIEEL is a hybrid mechanism of chemiluminescence and fluorescence and can produce red-shifted luminescence for better tissue penetration, CIEEL was also investigated for its potential applications in live animal imaging. As many small chemiluminescent substrates are known to react with ROS while still having good biodistribution characteristics, it is feasible to develop a viable CIEEL strategy for imaging tissue inflammation in living animals. Nevertheless, a critical challenge would be on the fluorescent energy recipient side. Since CIEEL requires close proximity of the chemical energy donor and the fluorescent recipient to ensure efficient energy transfer and light production, any ROS-sensing CIEEL strategy would need to achieve specific accumulation of both the ROS-sensing chemical

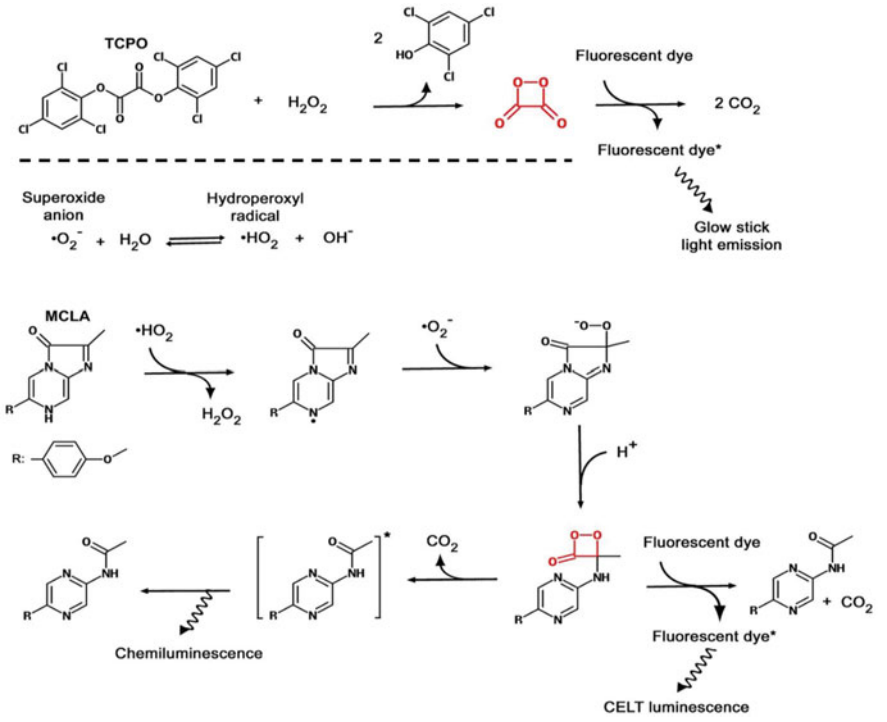

Fig. 7 Glow stick chemistry and CIEEL energy transfer mechanism of MCLA. Common commercially available glow sticks utilize TCPO as the energy source to produce CIEEL energy transfer luminescence. TCPO reacts with hydrogen peroxide to produce 1,2-dioxetanedione (in red), a high-energy intermediate. In the presence of a fluorescent recipient, the chemical energy can be transferred via formation of a charge-transfer complex of the intermediate and the fluorescent recipient. If no fluorescent recipient is present, the high-energy intermediate self-decomposes into two molecules of carbon dioxide and releases its energy as UV emission or heat dissipation. The color of a glow stick is solely determined by the fluorescent recipient, making it possible to produce glow sticks in a variety of colors using the same chemical substrate. However, TCPO is not water soluble and therefore it is not suitable for biological applications. MCLA is a methylated *Cypridina* luciferin analog that has several properties suitable for in vivo applications. The compound is small and has no net charge, allowing for penetration of both plasma membrane and membranes of subcellular organelles. Importantly, MCLA readily reacts with superoxide or its downstream ROS derivatives such as the hydroperoxyl radical to form a high-energy 1,2-dioxetane intermediate capable of CIEEL energy transfer in a mechanism similar to TCPO

energy donor and the fluorescent energy recipient at the same microscopic localization. This is a rather difficult task to achieve in living animals.

To overcome the proximity issue, a straightforward approach for CIEEL is to pack the chemical donor together with the fluorescent recipient in microbeads or nanoparticles. This will ensure activated chemical compounds have sufficient opportunity to collide and transfer their energy to fluorescent dyes. In a sense, this strategy is very similar to using miniaturized glow sticks for ROS imaging. In vivo imaging

using these miniature glow sticks in living subjects has also been tested and good progress has been made for inflammation imaging. For example, although the poor solubility or TCPO prohibits its direct application in in vivo imaging, Lee et al. have demonstrated that nanoparticles formulated from peroxyoxalate polymer and a fluorescent dye were capable of sensing hydrogen peroxide and generating far-red CIEEL luminescence in living animals [65]. Similarly, other types of small peroxyoxalate-based chemiluminescent substrates that are sensitive to ROS and singlet oxygen have been packed into larger polymer-based nanoparticles or microbeads for CIEEL applications.

An alternative CIEEL strategy to achieve concentrated co-localization of both the donor and recipient is to take advantage of the naturally formed small ROS-producing cellular compartments. In inflamed tissues, one of the suitable compartments is the phagosome in stimulated phagocytes. For the choice of CLI energy donor for this CIEEL strategy, in addition to having good ROS reactivity, the substrate also needs to be small and membrane-permeable to reach intracellular phagosomes. In this regard, TCPO is not suitable for this strategy due to its poor water solubility. Luminol, despite its usefulness for imaging of MPO activity, seems to have a very unstable intermediate state and thus is more suitable for CRET [66]. MCLA, on the other hand, has several characteristics suitable for in vivo CIEEL applications [45]. MCLA is a *Cypridina* luciferin analog and has good solubility and stability in aqueous solution. Importantly, this substrate can readily react with superoxide or its downstream ROS derivatives [67] to form a high-energy 1,2-dioxetane intermediate similar to TCPO (Fig. 7). MCLA is uncharged and relatively small (MW = 291.7), enabling it to penetrate both the plasma membrane and membranes of subcellular organelles. Additionally, MCLA does not undergo redox cycling when reacting with ROS. The in vivo proof of concept for this subcellular compartment CIEEL imaging strategy is shown in Fig. 8. Phox-specific CIEEL light can be produced by selective targeting of ROS-producing phagosomes by fluorescent dyes. These highly accumulated fluorescent dyes then serve as CIEEL energy recipients for MCLA [68]. Interestingly, MCLA CIEEL imaging can also be used to visualize other organelles that produce endogenous ROS. For example, by using mitochondria-targeting fluorescent dyes, it is possible to visualize ROS produced in mitochondria during oxidative phosphorylation. Besides CIEEL imaging of ROS production, this strategy could be extended to visualize other endogenous hydrolytic enzyme activities in living animals by replacing ROS-sensitive substrates with substrates that can be activated by specific enzymes [69]. Several metastable 1,2-dioxetane compounds have been engineered with protective groups to prevent their activation. These protective groups can be removed by hydrolytic enzymes such as β-galactosidase and alkaline phosphatase [61]. Once activated with a suitable enzyme, the chemical energy within the activated substrate can be transferred to a nearby fluorescent recipient via the CIEEL mechanism.

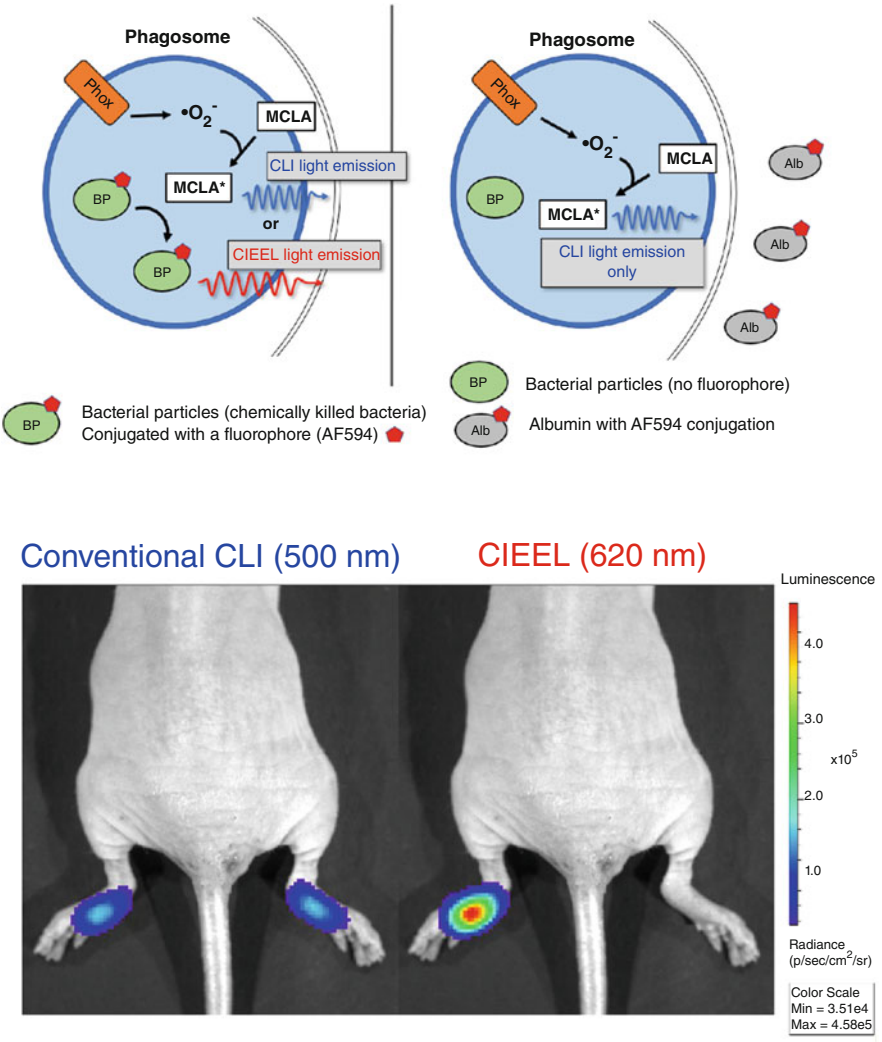

Fig. 8 In vivo CIEEL inflammation imaging using small fluorophores as energy recipient. *Top row*: in this set of footpad inflammation study, we tested whether MCLA is capable of CIEEL energy transfer to the fluorescent recipients conjugated to the bacterial particles (BP). *Bottom row*: subcutaneous injection of Alexa Fluor 594-labeled bacterial particles (BP-AF594) in the left footpads triggered rapid phagocyte accumulation and phagosome ROS production. As controls, the right footpads received a mixture of unconjugated BP and Alexa Fluor 594-labeled albumin (BP + Alb-AF594). As albumin is a common serum protein lacking pathogenic molecular signatures, the phagocytes preferentially engulfed BioParticles but not the Alb-AF594 conjugates. In the footpads receiving BP-AF594, we observed good CIEEL emission (620 nm) using the IVIS® Spectrum imaging system after intravenous delivery of MCLA, indicative of high levels of energy transfer to the AF594 moiety. In contrast, control footpads only produced conventional blue chemiluminescence (500 nm) but very low CIEEL emission from the AF594 moiety on Alb-AF594 (620 nm). Images shown are original data from an unpublished study

3 Noninvasive Fluorescence Imaging for Tissue Inflammation

In comparison to CLI, fluorescence imaging (FLI) is a more mature technology that has been widely used for preclinical small animal imaging [70]. Instead of using chemical energy stored within low molecular weight substrates, FLI uses an external light source to excite the fluorophore. Therefore, FLI has a simpler, robust, and straightforward workflow making it more flexible when choosing the right fluorescent probes to suit the research need. It is also possible to perform multicolor imaging on the same animal using probes of different fluorescent wavelengths. The spectral range of FLI is limited by background signals observed from two major sources: tissue autofluorescence at visible wavelengths (peaking at ~500 nm) and interfering mouse chow fluorescence (primarily due to chlorophyll and peaking at ~680 nm). Fortunately, these interfering background signals can be mostly avoided by using NIR-shifted fluorophores and by feeding mice low-fluorescence chow. Therefore, the optimal FLI operates in the range from red to NIR spectra (650–850 nm). Another consideration is the inherent short Stokes shift (~20–40 nm) of most dyes that can modestly decrease fluorescent output due to the requirement of filtering out the emission/excitation overlap [39]. Nevertheless, since the power output for the excitation light is tunable, FLI techniques have a more intense signal output than small chemical compound-based CLI in general. Of note, since modern FLI operates in the red or NIR spectra, it is not hindered by the blue chemiluminescence issue associated with small CLI compounds; recent developments and advances in optical imaging reagents and instrumentation have made FLI more attractive for deep tissue imaging than CLI. This advantage also makes FLI techniques more likely to be translated into clinical use. Various red and NIR fluorescent probes are commercially available for imaging small animals. In addition to planar 2D images, when combined with sufficiently strong excitation light sources such as NIR lasers or halogen lamps coupled with NIR filters, FLI offers sufficient tissue penetration and probe excitation in small laboratory animals to generate 3D tomography images. For example, fluorescent molecular tomography (FMT®) systems that are equipped with strong transilluminating NIR lasers are capable of deeper tissue penetration and faster 3D reconstruction for whole-body imaging in small laboratory animals. Schematic diagrams explaining the difference between the conventional 2D planar and 3D tomographic FLI imaging techniques are provided in Fig. 9.

Aside from imaging instrumentation, the accessibility of a wide range of fluorescent probes also plays a key role in the success of FLI. Traditionally, FLI probes are designed to directly bind/target specific biological markers and pathological features involved in tissue inflammation. The smaller, fluorescently active moiety can be conjugated to a larger targeting agent such as a peptide or protein (antibody). In a sense, FLI probes behave like drugs or therapeutical biologicals of comparable sizes, and their pharmacokinetic and pharmacodynamic properties need to be considered

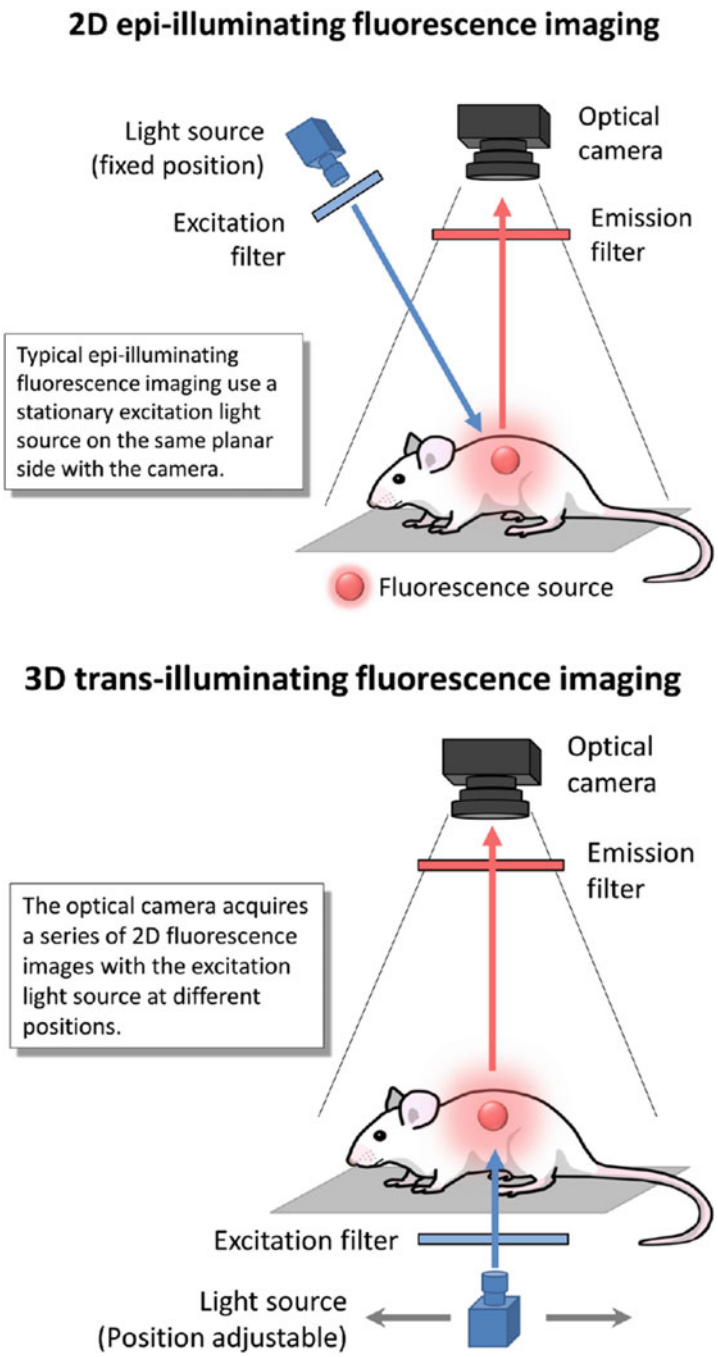

Fig. 9 Instrumental schematics of 2D and 3D FLI imaging. There are two types of FLI imaging for small laboratory animals. The first type is the conventional 2D epi-illumination FLI (*top*). In this configuration, both the excitation light source and the camera are on the same planar side with respect to the animal subject. The advantage of using a stationary epi-illumination light source is to

for successful in vivo imaging applications. In the following sections, we will discuss the major FLI probe design strategies for inflammation imaging.

3.1 Targeting Enhanced Vascular Permeability at Inflamed Sites

One of the hallmarks of local inflammation is tissue swelling (edema), characterized by excess fluid buildup in the injured tissues. This phenomenon is caused by local inflammatory signals such as prostaglandins which increase vascular permeability to facilitate leukocyte infiltration and erythema formation. In addition to cellular extravasation, vascular leakiness and tissue swelling result in enhanced permeability and retention (EPR) for large molecules with sizes greater than 16 kDa [71]. Several fluorescent probes and nanoparticles have been developed to systemically visualize leaky vasculature and have been widely used to visualize edema and vascular leakiness in inflamed tissues [72]. Figure 10 illustrates the polymer-based and nanoparticle-based designs of FLI probes for vascular and inflammation imaging. Typically, these probes differ in size and can have a variety of blood half-lives and speed of extravasation into tissue, though longer circulation times facilitate leakage into sites of chronic swelling and inflammation. Therefore, this type of vascular FLI probe can be injected into animals and imaged immediately to visualize general tissue vasculature in both healthy and diseased tissues. After a period of incubation, the probes will extravasate and accumulate in the inflamed tissues to generate inflammation-specific signals. Figure 11 demonstrates the use of these two types of FLI probes for imaging inflammation in a mouse model of arthritis. Of note, this class of probe does not target a specific molecular feature (e.g., enzymes, markers) in the inflamed tissue, and the accumulation is based on increased vascular permeability, although non-targeting nanoparticles can be further engulfed by macrophages [73]. Nevertheless, these probes can be used not only to systemically scan the whole

Fig. 9 (continued) cast the excitation light over multiple animal subjects and therefore increase operational throughput. However, as excitation light is spread over a larger area, planar 2D FLI is typically not suitable for imaging fluorescent targets deeper than 5 mm. The second and more advanced type is 3D transillumination FLI (*bottom*). Unlike conventional 2D FLI, the excitation light source is placed on the opposite site of the imaging plane and under the animal subject with respect to the camera. Of note, the transilluminating light source is not stationary. For a typical 3D FLI imaging, the light source needs to be placed at various positions near the fluorescent target, and the positional variation of fluorescent signal is the basis for 3D tomographic reconstruction. The advantage of this configuration is better tissue penetration as the intense focal excitation source is placed underneath the subject and close to the fluorescent target. For example, the laser-based FMT system can have tissue penetration in the range of 30–40 mm depending upon the laser power and NIR wavelength. However, as multipoint excitation is required, tomography 3D FLI is generally slower and has lower throughput than the planar 2D FLI, requiring algorithmic reconstruction

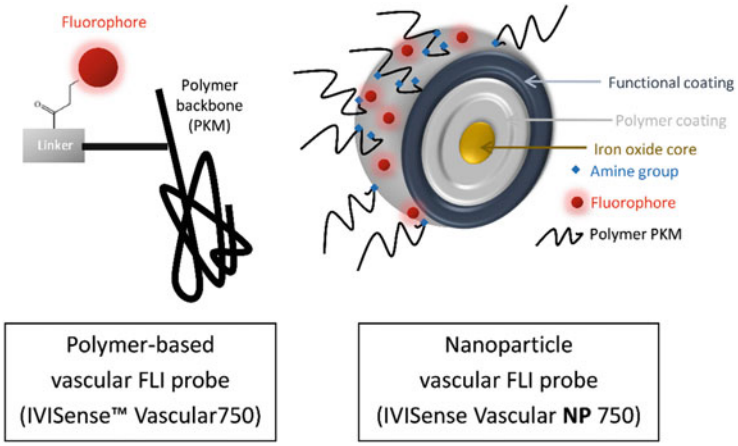

Fig. 10 Design schematics of circulating vascular FLI probes. Polymer-based fluorescent probes *(left)* and nanoparticle-based *(right)* FLI probes with good blood pool stability can be used to visualize general tissue vasculature in both healthy and diseased tissues. Interestingly, after a period of incubation, these probes will extravasate and selectively accumulate in the edematous tissues since local inflammatory signals cause increased vascular leakiness. For example, a polymer-based vascular FLI probe, IVISense Vascular 750 (also reported as AngioSense® 750), has a long polymer backbone that serves as a pharmacokinetic modifier (PKM) for enhanced blood stability. A NIR fluorophore can be chemically conjugated to the backbone via a linker. Another vascular FLI probe design is based on nanoparticles. For example, a nanoparticle vascular FLI probe, IVISense Vascular NP 750 (also reported as AngioSpark® 750), has a metal oxide core and contains layers of polymer and functional coating. To enhance its blood stability, the surface is modified with polymer PKMs. In addition, the fluorescent signals are generated by NIR fluorophores conjugated to the surface functional coating. The PKM modification prolongs the particles' circulation time without affecting their intense NIR fluorescence. Although neither FLI probe targets a specific inflammatory molecular feature (enzymes, markers), both are selectively retained within the inflamed sites due to the unique pathological feature in inflamed tissues (e.g., leaky vasculature and erythema). Nevertheless, their selective retention in inflamed tissues makes it possible to systemically scan the whole body to pinpoint the inflammation sites

body to pinpoint inflammation sites but also to provide a quantitative means of assessing their inflammation status.

3.2 Selective Binding and Targeting of Inflammatory Protein Markers

This is the most straightforward and robust design concept for inflammation FLI probes: designing a fluorescent probe that is capable of direct interaction and binding to a specific inflammatory marker. Targeted fluorescent probes can be delivered systemically into animals to bind upregulated inflammatory markers, thereby accumulating at sites of disease. Figure 12 illustrates three examples taking advantage of

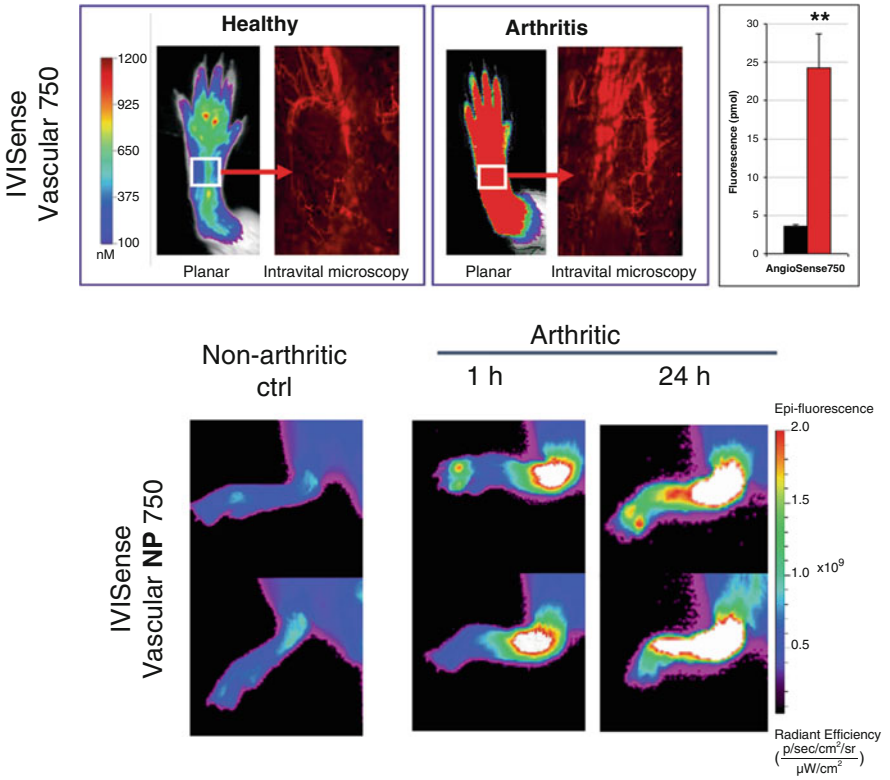

Fig. 11 FLI of vascular leakiness associated with inflammation in an arthritis mouse model. Collagen antibody-induced arthritis (CAIA) was induced by antibody cocktail injection, and mice with CAIA arthritis were used in this set of studies. Increased vascular permeability in the arthritic tissues was visualized by polymer-based FLI probes (IVISense Vascular 750, *top*) and nanoparticles (IVISense Vascular **NP** 750, *bottom*). Both FLI probes with good blood pool stability can be injected into animals and visualize general tissue vasculature in both healthy and diseased tissues. After systemic delivery of IVISense Vascular 750, 2D planar FLI and intravital microscopy were performed immediately to confirm enhanced vasculature development in the CAIA footpads. The 2D FLI signals can be quantified for a more accurate assessment of the inflammation status (**$P < 0.01$). The presence of IVISense Vascular 750 in vasculature was also validated by intravital microscopy (arrows). In another set of studies, IVISense Vascular NP 750 nanoparticles were systemically injected into non-anthric and CAIA mice. The mice were imaged at 1 and 24 h after nanoparticle injection. Significantly increased inflammatory FLI signals were observed at 1 h in the CAIA footpads, where fluorescent signals further increased at 24 h after more particles extravasated and were retained in the inflamed tissue. Selective extravasation and retention of nanoparticle signals in the inflamed tissues is largely caused by increased vascular leakiness. Images shown are original data from unpublished studies

known ligand interactions with their inflammation biomarkers. This type of probe can also be used in vitro for imaging cells and for ex vivo imaging of tissues to validate specific targeting in animals.

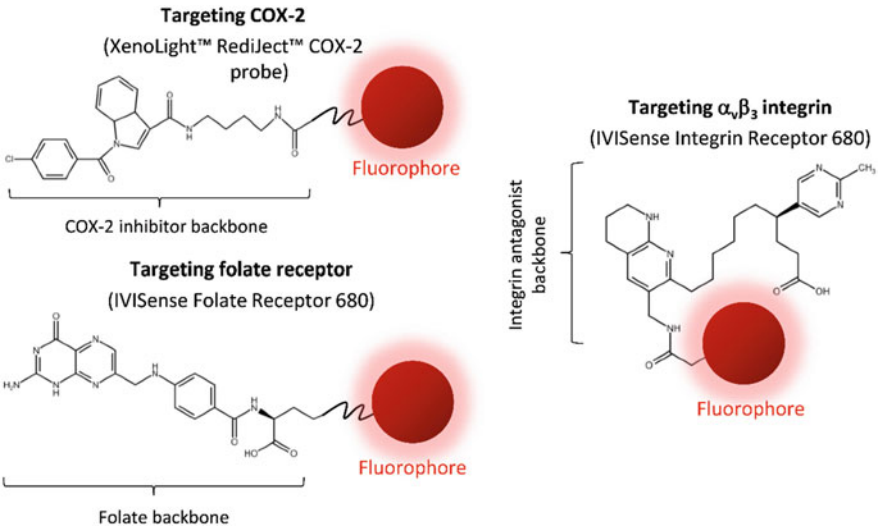

Fig. 12 FLI probe designs for direct targeting inflammatory markers. FLI probes can be designed to directly interact and bind to specific inflammatory markers. This can be achieved by using known small moieties that specifically interact and bind to the protein targets. For example, small COX-2 inhibitors that show excellent specificity and binding affinity can be used as targeting backbones to which a NIR fluorescent moiety is chemically liked (XenoLight™ RediJect™ COX-2 probe). Similar strategies can be used to produce a FLI probe directly targeting folate receptors or integrin αvβ3 by taking advantage of their known binding partners, folate (IVISense Folate Receptor 680, also reported as FolateRSense™ 680) or an RGD mimetic αvβ3 antagonist (IVISense Integrin Receptor 680, also reported as IntegriSense™ 680)

One of the best examples of this strategy is cyclooxygenase-2 (COX-2)-targeting fluorescent probes. COX-2 is an attractive biomarker for inflammation. Although COX-2 expression is also found in a healthy tissue, its expression in macrophages is highly upregulated in inflamed and malignant tissues [74]. COX-2 is a cytosolic enzyme that catalyzes the conversion of arachidonate, an essential fatty acid, to prostaglandins, which are involved in modulating vessel permeability and inflammatory responses. COX-2 expression is typically low or undetectable in most healthy tissues. However, COX-2 activity at sites of inflammation is highly upregulated. COX-2 has also been shown to play a central role in tumorigenesis in various carcinomas. Figure 13 demonstrates the use of a COX-2-targeting probe for FLI of tumor-associated COX-2 expression.

Because of its critical role in promoting inflammation, inhibition of COX-2 can provide relief from symptoms of inflammation and pain. Several small COX-2 inhibitors have been developed as nonsteroidal anti-inflammatory drugs (NSAIDs) that show excellent specificity and binding affinity. Taking advantage of these small inhibitors as backbones, a series of COX-2-specific fluorescent probes were designed and synthesized. A red or NIR fluorescent moiety (such as rhodamine) can be chemically liked to the targeting moiety that is based on the inhibitor backbone. Although the final structure (Fig. 12) is larger than the original inhibitor

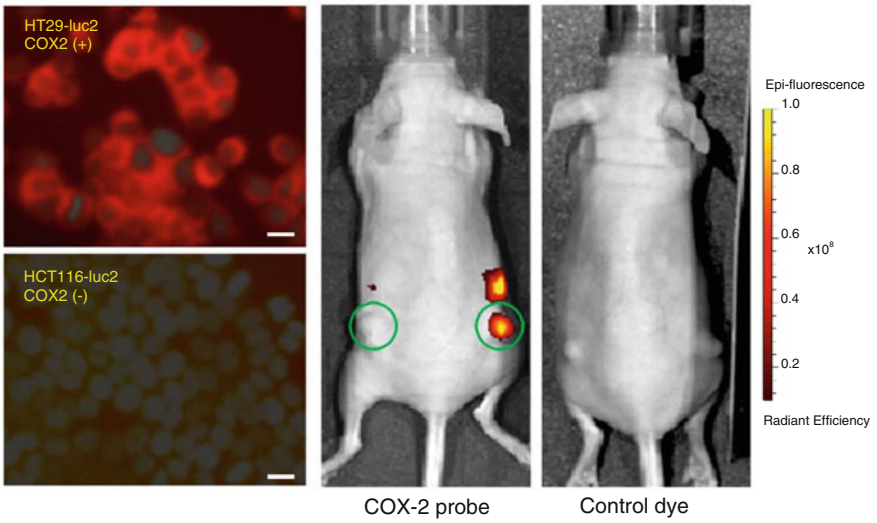

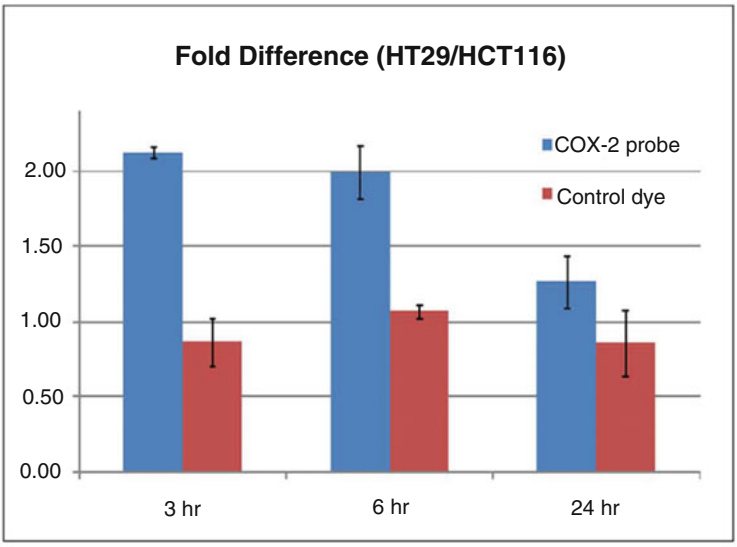

Fig. 13 Direct targeting of COX-2 expression in cancer cells. Cyclooxygenase-2 (COX-2) is an inflammatory biomarker known to be expressed in macrophages as well as in malignant tumors. In cultured cells *(top left)*, a COX-2-specific FLI targeting probe (XenoLight RediJect COX-2 probe) can bind to the COX-2-positive HT29 cells, but not to HCT116 cells (scale bar: 10 μm). IVIS® Spectrum imaging *(top right)* of mice bearing both a subcutaneous HT29 tumor (right flank) and a HCT116 tumor (left flank) revealed specific COX-2 targeting only in the COX-2-positive HT29 tumors. A control dye lacking the COX-2 targeting moiety showed low fluorescence in both tumors (*bottom graph*; mean ± s.e.m.). Images shown are original data from an unpublished study

backbone, the endogenous substrate of COX-2, arachidonate, is a long-chain fatty acid, and therefore the enzyme is able to accommodate the elongated fluorescent moiety without losing much of its binding affinity and specificity.

Similar design strategies can be adopted to target other inflammation-specific proteins/markers that have well-characterized "activity pockets" for the targeting moiety to interact and bind. The goal of this generalized strategy is to conjugate a fluorescent dye to the targeting moiety in such a way that the dye does not interfere with the targeting moiety's physical interaction with the activity pocket. For enzymes, the targeting moieties can be their substrates or specific inhibitors. For surface receptors, the targeting moieties can be its ligand or specific antagonists. Appropriate spacer groups or linkers may be needed between the dye and targeting moiety in order to prevent steric hindrance during binding. For instance, folic acid has emerged as a good direct targeting ligand backbone for inflammation FLI. Folate receptors (FRs) have three isoforms (α, β, γ) in humans, and their expression is mostly restricted to inflammatory macrophages and cancer cells to accommodate the increased energy consumption and metabolism of these cells [9]. Specific fluorescent imaging probes have been developed to image arthritis and acute lung inflammation mouse models [75, 76]. The success of this particular design strategy is due to the facts that folate is a relatively small (MW = 441.4) and linear molecule and that its binding pocket in FRs is large enough to accommodate the additional fluorophore with minimal detrimental effects on binding affinity. In fact, similar conjugation schemes have been used to deliver anticancer drugs for selective targeting of tumor cells with high levels of FR expression. After specific binding to cell surface FR, the fluorescent or drug conjugates are internalized via endocytosis which further enhances fluorescent contrast. In principle, this design strategy is not specific to FRs and has been extended to target other cell surface receptors that are known for their recycling and trafficking between the plasma membrane surface and the intracellular endomembrane systems [77, 78].

Some types of integrins are also good imaging targets for inflammation imaging. Integrins are a family of αβ heterodimeric receptors that comprise 24 αβ pairs with multiple conformations and interact with a wide variety of components in the extracellular matrix (ECM). They can modulate their binding affinity through conformational switches. As they bridge the extracellular matrix and intracellular cytoskeleton, integrins play critical roles in bidirectional signaling across the plasma membranes involved in many biological processes, such as inflammation, angiogenesis, cell survival, and tumorigenesis [79]. Integrin αβ dimers can be categorized into four classes: leukocyte, collagen-binding, Arg-Gly-Asp (RGD)-binding, and laminin-binding. In particular, the RGD-binding integrin αvβ3 is of great interest as it is involved in many inflammatory processes. Integrin αvβ3 is known to be expressed on differentiated macrophages and angiogenic endothelial cells to regulate vascular permeability [10, 80]. Integrin αvβ3 is also highly expressed on rapidly growing cells under pathological conditions such as cancer, while its expression is typically minimal on quiescent normal cells [81]. Therefore, integrin αvβ3 is a good biomarker for imaging vascular inflammation using various probes and imaging modalities [11, 82–84]. Figure 14 illustrates the use of a fluorescent targeting probe

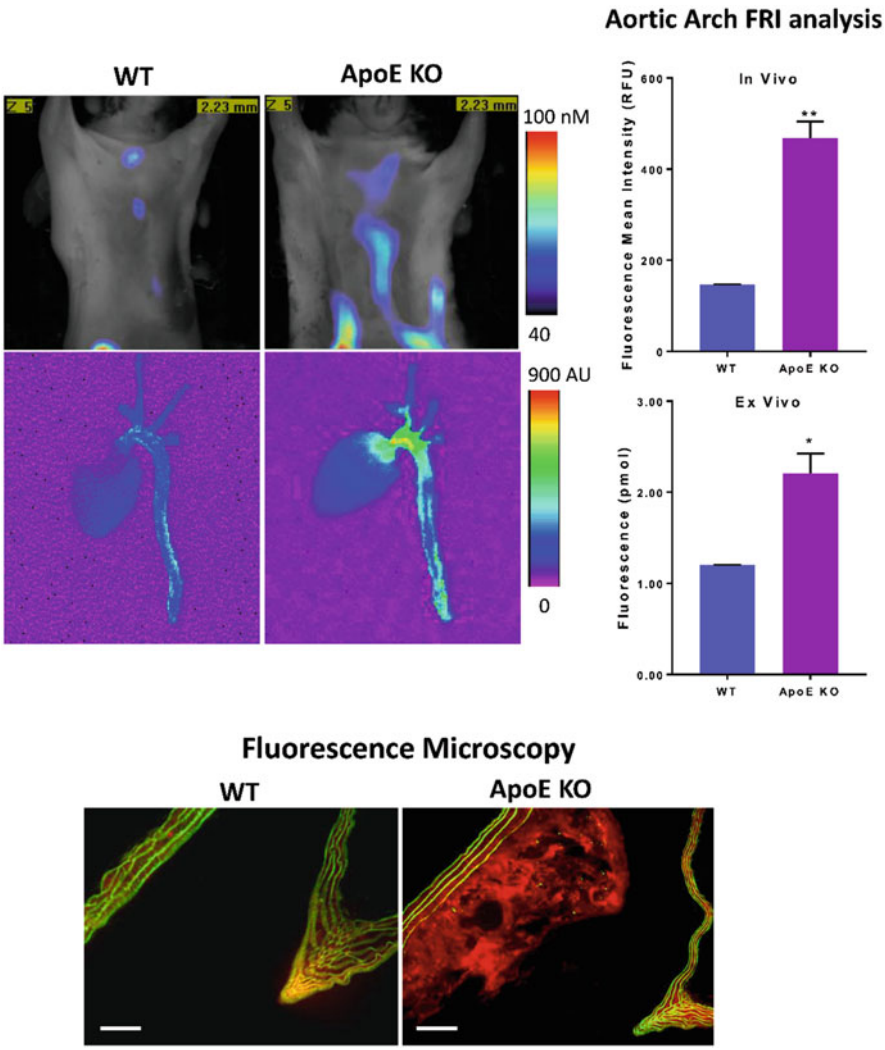

Fig. 14 Direct targeting of integrin expression in a mouse model of atherosclerosis. Atherosclerosis in ApoE$^{-/-}$ male mice was induced by feeding with high cholesterol diet for 16–18 weeks. To visualize plaque formation in living animals, the ApoE$^{-/-}$ and age-matching C57BL/6 wild-type mice were injected i.v. with 8 nmol of IVISense Integrin Receptor 680 probe, and specific integrin signals were imaged 48 h later *(top left panels)*. Following imaging, mice were sacrificed and perfused with PBS. The heart, aortic arch, and descending aorta were excised and ex vivo 2D planar FLI were performed. In addition, the tissues were subject to fluorescence microscopy, and higher level of integrin expression (*bottom images*, in red) was observed in the aortic plaque in the ApoE$^{-/-}$ mouse (scale bar: 100 μm). The green color represents the autofluorescence of collagen. Images shown are unpublished original data consistent with a related published study [85]

specific to integrin αvβ3 to visualize chronic inflammation in the ApoE$^{-/-}$ atherosclerosis mouse models [85]. In this example, the ApoE$^{-/-}$ mice were maintained on high cholesterol diet for 16–18 weeks to induce atherosclerosis. Systemic delivery (i.v.) of IVISense Integrin Receptor 680 probe detected higher integrin levels in association with plaque formation in the ApoE$^{-/-}$ mice. Subsequent ex vivo imaging and fluorescence microscopy studies confirmed the in vivo imaging findings.

3.3 *ROS-Reactive Fluorescent Probes for Inflammation Imaging*

In the previous sections, we discussed the use of small, ROS-reacting compounds to selectively target inflamed tissues for direct CLI imaging. Another parallel strategy for FLI is to use small compounds whose fluorescence properties can be "turned on" or altered by reacting with ROS in pathophysiological environment. For tissue and cell staining and microscopic imaging, several reaction-based fluorescent probes have been developed to visualize ROS and other reactive nitrogen and sulfur species [86]. In addition, ROS-sensing fluorescent probes have been widely used to image ROS production in plants to study their response to environmental and developmental changes [87]. Successful ROS sensing in living animals has been performed using a hydrocyanine-based fluorescent probe [88], and this strategy has shown promising proof-of-concept results for visualizing inflammatory ROS production and oxidative stress in rodent retina [89]. However, other classes of ROS-reacting FLI probes have had limited success since most of these ROS-reacting fluorescent probes operate in the green spectral range that is not ideal for imaging live animals. Green-fluorescent probes are still useful for superficial imaging, e.g., for image-guided surgery [90]. Nevertheless, some red ROS-sensing fluorescent imaging probes can be delivered locally to visualize inflammation caused by biomaterial implants in living subjects [91]. Their highly reactive nature makes them poorly stable after systemic injection into animals and might have long-term safety and toxicity implications. To address this, recent developments in ROS-sensing FLI have focused on polymer-based nanoparticles or liposome-based micelles to encapsulate the reactive dyes [92]. Semiconducting polymer dots (Pdots) have also shown promising results for ROS-sensing FLI of hypochlorous acid (HOCl) in mice [93].

3.4 *Activatable Fluorescent Probes for Imaging Specific Inflammatory Protease Activity*

Using protease-activated fluorescent probes is by far the most successful and widely used FLI strategy for inflammation imaging [94–96]. This strategy has several advantages over the blood-pool/edema, biomarker direct-binding, and

Table 1 Examples of peptide motifs that can be used to develop activatable probes specific for inflammatory proteases

Protease	Peptide motif
Neutrophil elastase	PMAVVQSV
Matrix metalloproteinase-2/-9 (MMP-2, MMP-9)	GPPGVVGEKGEQ
Cathepsin B (Cat B)	GFLG

ROS-sensing FLI probes. By selectively targeting unique protease activities such as neutrophil elastase, MMPs, and cathepsins (see Sect. 1.4 and Table 1) in inflamed tissues, protease-activated fluorescent probes have much higher specificity than the nonselective blood-pool/edema imaging probes. These probes also show lower background signal and thus better signal-to-noise ratios than "always-on" targeted probes, since probes in normal tissue that are not activated by protease activity do not emit fluorescent light.

Figure 15 illustrates the working principles of protease-activated fluorescent probes. This type of probe is designed to take advantage of the self-quenching property of fluorescent dyes: when two or more near-infrared fluorescent (NIRF) dyes are placed in close spatial proximity, the energy of absorbed excitation light is released in the form of heat due to energy transfer between the dye molecules. Figure 16 illustrates two fluorescent probe designs for imaging pan-cathepsin activity. The first design consists of a large polypeptide scaffold and multiple dye moieties (standard IVISense Pan Cathepsin 680, also reported as ProSense 680). By conjugating NIRF dyes to a long-circulating graft copolymer backbone consisting of poly-L-lysine, the proximity of the dyes to each other results in an internally quenched probe. However, in the presence of a suitable protease, the peptidyl backbone can be cleaved to release the fluorescent dyes. The separated, unquenched dyes are now capable of producing fluorescent signals. Therefore, the larger scaffold version has delayed but stronger fluorescence in response to the target protease activity. On the other hand, the small scaffold version (IVISense Pan Cathepsin 750 FAST, also reported as ProSense® 750 FAST) has a short but more enzyme-specific peptide linking only a pair of quenched fluorophores. The smaller size makes it faster for tissue delivery and penetration. In addition, the more unique and specific peptidyl sequence enables quicker digestion in response to protease activation. The peptidyl backbone can be further modified with a pharmacokinetic modifier (PKM) such as methoxy polyethylene glycol (mPEG) to fine-tune the probe's biodistribution properties in living animals [94, 95].

This versatile platform makes it possible to design and produce a variety of protease-specific FLI probes. For example, several activatable probes have been developed to target proteases with significant roles in inflammation, including neutrophil elastase [97], matrix metalloproteinases [98], and cathepsins [99]. Examples of peptide motifs recognized by these proteases are provided in Table 1. Several studies have demonstrated the effectiveness of this strategy to image inflammatory protease activities in living subjects. For example, using this strategy, specific neutrophil elastase activity was noninvasively visualized in early atherosclerotic

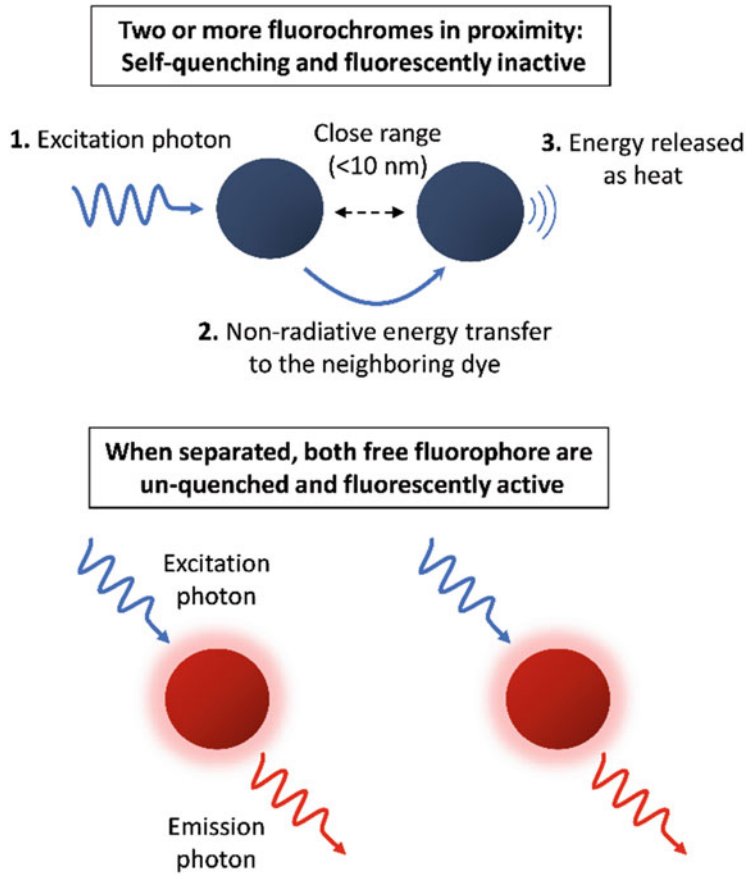

Fig. 15 Self-quenching of fluorescent dyes in close proximity. Fluorescent quenching can occur when two or more of the same fluorophores are in close proximity. As both molecules have the same excitation/emission spectral spectra, when they are in close range (<10 nm), the energy absorbed by one fluorophore can be non-radiatively transferred to the neighboring fluorophore. This type of dynamic quenching is based on the FRET mechanism. However, there is no emission from the recipient and the energy is eventually released as heat. Importantly, the quenching process is distance-dependent. When both fluorophores are separated and free of interference from each other, they are fluorescently active and capable of emitting light after excitation

lesions in a mouse model [100]. In an experimental murine asthma model, a pan-cathepsin activable FLI probe was used to detect eosinophils and monitor treatment responses to dexamethasone [101]. An MMP-specific FLI probe was able to detect early joint inflammation in a collagen antibody-induced arthritis (CAIA) mouse model [102]. Figures 17 and 18 show examples of successful FLI of various inflammatory protease activities in a similar CAIA mouse model [103]. Systemic whole-body imaging reveals strong NE activity in the joints of forepaws, knees, and hind paws (Fig. 17); the algorithms of the applied FMT system

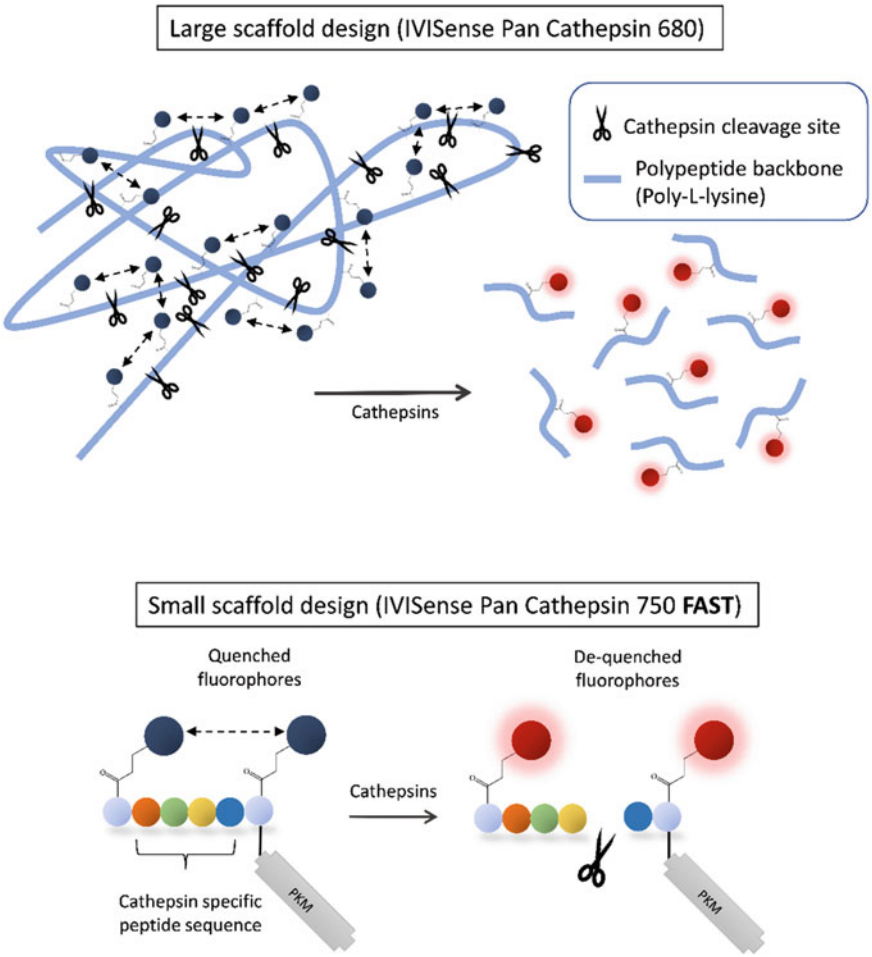

Fig. 16 Schematic diagrams of protease-activated FLI probes. Many fluorescent dyes are self-quenching and when two or more dyes are placed in spatial proximity, they do not emit fluorescent light. Taking advantage of this property, the quenched state can be achieved by linking two fluorescent dyes with a peptide scaffold that is susceptible to a specific protease activity. When the target protease is present, the scaffold is cleaved, and the released fluorescent dyes become fluorescently active. This strategy can be used to generate a variety of protease-sensing FLI probes by selecting different, target-specific peptide sequences. In addition, the pharmacokinetic characteristics can be fine-tuned with the length of the peptide scaffold or with PEG-based polymers (PKM, pharmacokinetic modifier). For example, depending on the length of the peptide scaffold, two versions of cathepsin-specific activatable probes can be prepared. The larger scaffold version (standard IVISense Pan Cathepsin 680, also reported as ProSense 680; *top*) has higher molecular weight and contains multiple dye moieties. Therefore, the larger scaffold version has delayed but stronger fluorescence in response to the target protease activity. On the other hand, the small scaffold version (IVISense Pan Cathepsin 750 FAST, also reported as ProSense® 750 FAST; *bottom*) has a short and more specific peptide linking only a pair of quenched fluorophores. This design makes it faster for tissue delivery and penetration, and therefore quicker to respond to protease activation. The short version also contains a pharmacokinetic modification such as mPEG to improve its blood stability and biological viability

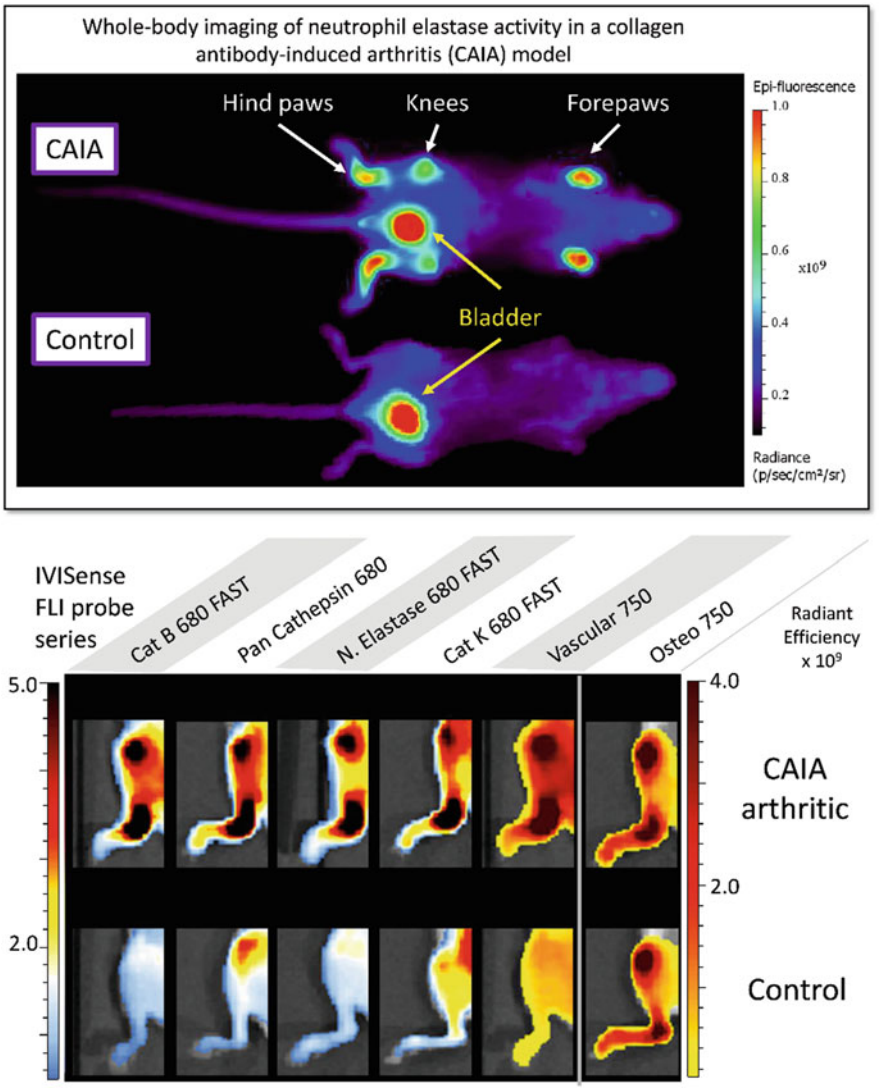

Fig. 17 Protease-activated FLI probes for imaging arthritic tissues**.** Collagen antibody-induced arthritis (CAIA) was induced by antibody cocktail injection. Whole-mouse 2D planar FLI *(top)* using the IVIS® Spectrum imaging system shows specific accumulation of a neutrophil-specific NIR imaging probe (IVISense Neutrophil Elastase 680 FAST, top panel) in the CAIA arthritic mouse at the peak of inflammation. The arrows indicate regions associated with either inflammation at joints (white arrows) or probe clearance via the renal/bladder path (yellow arrows). The lower panels show a range of protease-activatable imaging probes that detect inflammatory changes in the knees and ankles of CAIA mice. Compared to disease-negative controls, elevated inflammatory protease activities were observed including cathepsins (IVISense Cat B/K 680 FAST, IVISense Pan Cathepsin 680) and neutrophil elastase (IVISense Neutrophil Elastase 680 FAST). In addition, the edema in the inflamed knees and ankles also caused higher vascular leakiness and higher retention of IVISense Vascular 750. Of note, there was no difference in IVISense Osteo 750 (also reported as OsteoSense™ 750) signals as both CAIA and normal joints at the peak of inflammation are

allow for quantitative assessment of treatment responses in this CAIA model (Fig. 18).

4 Conclusion

Although in this review we have discussed CLI and FLI as two separate approaches for noninvasive optical imaging of tissue inflammation, in practice, modern optical imaging instruments are equipped with highly sensitive camera systems and high-performance filter sets and can simultaneously perform CLI and FLI on the same animal subject. The quantitative nature of both CLI and FLI makes optical imaging a highly valuable, complementary modality to CT, MRI, and ultrasound whose strengths are in anatomical and structural imaging. In addition to appropriate imaging instrumentation, the key to successful inflammation imaging is the luminescent probe. As both CLI and FLI probes take advantage of unique features at various levels in the inflamed tissues, they define the inflammatory target specificity and biological readouts. At the tissue level, FLI probes are available to target edema and vascular leakiness. At the cell level, different CLI substrates can be used to distinguish neutrophils and macrophages based on their preference for different ROS production sites. Most importantly, at the molecular level, specific FLI probes can detect inflammatory protease activities that are critical in modulating immune responses and shaping inflammation outcomes in living animals.

As summary, Table 2 compares the pros and cons of these two optical imaging approaches. The fundamental difference of CLI and FLI is the energy source for light production. As CLI substrates are very sensitive to ROS produced by the inflammatory phagocytes, they have shorter incubation times and therefore can rapidly produce light signals after systemic delivery into animals. FLI probes typically require longer incubation times as they have more drug-like pharmacodynamic properties after systemic delivery. In order to generate sufficient fluorescence contrast, a period of time is needed for the FLI probe to specifically interact and accumulate at the inflamed site, while free FLI probes in the normal tissues are washed out and excreted via the renal or hepatic pathways. For CLI, there is currently a limited selection of small chemical compounds available for inflammation imaging. Furthermore, CLI is mostly limited to imaging inflammation at shallow locations: as most CLI substrates produce blue light after reacting with ROS, they are not ideal for imaging deep tissue and generally not able to produce 3D tomography images. On the other hand, FLI is a more versatile approach capable of targeting a great variety of physiological changes (e.g., leaky vasculature and EPR) and unique inflammatory biomarkers such as secreted proteolytic enzymes and

Fig. 17 (continued) expected to have similar levels of bone mineral turnover. Images shown are from unpublished studies

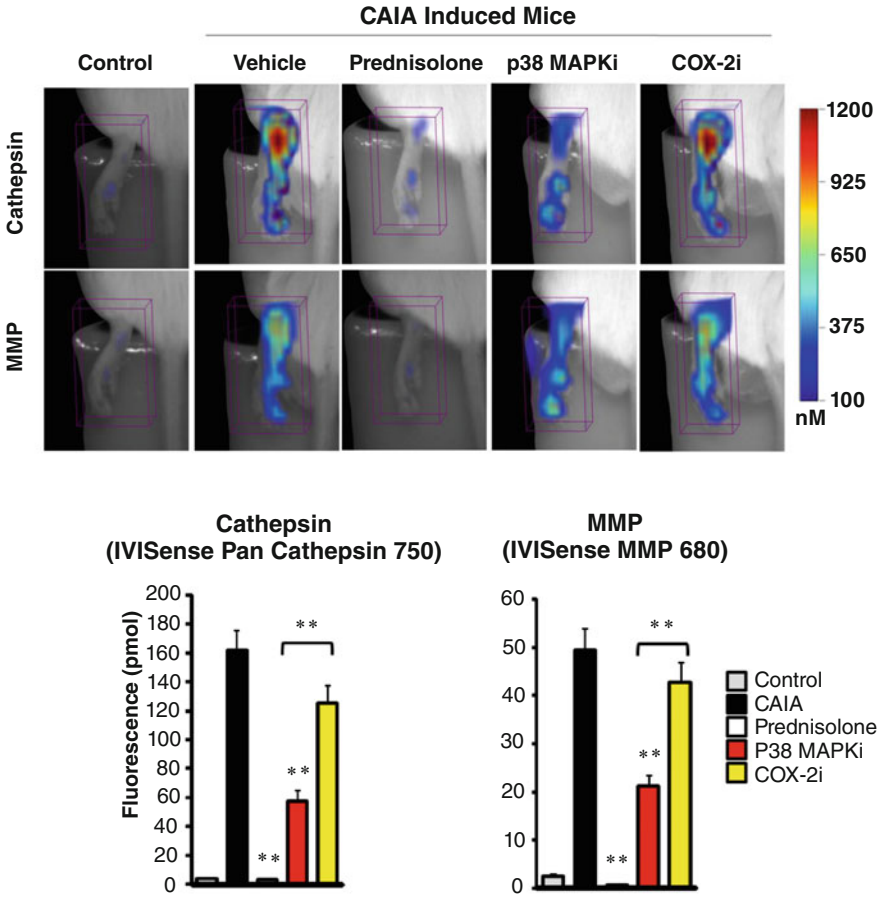

Fig. 18 Use of activatable FLI probes to image treatment responses in the CAIA arthritis model. The treatment responses of several anti-inflammatory drugs in the CAIA mouse model were visualized using the FMT® 4000 imaging system after systemic delivery of the pan-cathepsin (IVISense Pan Cathepsin 750) and MMP-specific (IVISense MMP 680, also reported as MMPSense™ 680) imaging probes *(top panels)*. Three anti-inflammatory drugs were tested in this study: prednisolone and inhibitors against p38 MAPK (P38 MAPKi) and COX-2 (COX-2i). Control joints have very low cathepsin and MMP activities, while the CAIA joints have elevated levels of both inflammatory proteases. The FMT® system used in this experiment allows quantification and enables accurate assessment of drug responses *(lower panels)*. In this example, prednisolone was the most effective therapy to suppress CAIA inflammation and protease activities. COX-2i only showed moderate anti-inflammatory effects in comparison to the untreated CAIA group (**$P < 0.01$, *t*-test). Images shown are original data from a related published study [103]

surface receptors. In particular, the most important advantage of FLI is that there are currently many NIR fluorescent probes available for deep tissue and 3D tomographic imaging. Table 3 summarizes all the FLI probes discussed in this chapter to provide a

Table 2 Comparison of CLI and FLI methods for inflammation imaging

Mode	Chemiluminescence (CLI)	Fluorescence (FLI)
Energy source	Chemical compounds activated by ROS	External excitation light
Advantages	• Highly sensitive to ROS produced by phagocytes • Fast reaction and light production after systemic delivery of small CLI substrates	• Versatile strategies to target inflammatory targets • Various NIR fluorescent dyes with different wavelength for deep tissue and 3D tomography imaging • Simultaneously imaging multiple targets at different channels • High light signal output • Mechanistic imaging of inflammation (protease, ROS possible)
Disadvantages	• Fewer choices of CLI compounds • Lower luminescence output compared with FLI • Mostly limited to 2D planar imaging: blue light produced by small CLI substrates are not suitable for deep tissue imaging • CRET and CIEEL energy transfer methods further reduce signal production efficiency	FLI probes have drug-like pharmacokinetic property, and therefore they require longer incubation time to circulate, interact, or activate in the inflamed tissues

broad overview of FLI imaging versatility and their potential applications in inflammation-related disease conditions such as cancer, arthritis, and atherosclerosis.

In the foreseeable future, with new discoveries and more knowledge obtained in inflammation biology, we expect great advances will be made in optical imaging. Recent proof-of-concept studies of CRET and CIEEL energy transfer nanoparticles greatly encourage the development of next-generation inflammation imaging probes. In return, these new probes could advance our understanding in this intricate, dynamic yet fundamental pathological process that is critical in so many human diseases.

Table 3 Selection of FLI probes mentioned and their applications

Type	Probe	Mechanism	Applications
Physiologic	IVISense Vascular750	IV circulation, EPR	Edema, cancer, arthritis, and other acute/chronic inflammation conditions
	IVISense Vascular NP 750	IV circulation, EPR	Vascular imaging of inflamed tissues by intravital microscopy
Targeted (direct-binding)	XenoLight RediJect COX-2 probe	COX-2 enzyme	Target upregulated COX-2 in cancer and other inflamed tissues
	IVISense Folate Receptor 680	Folate receptor	Tumor/inflammation metabolism marker; cancer, arthritis, and other acute/chronic inflammation conditions
	IVISense Integrin Receptor 680	Alpha V beta 3 integrin	Cancer (tumor and neo-vasculature), atherosclerosis (foam cells)
	IVISense Osteo 750	Hydroxyapatite	Bone turnover (growth and resorption): fracture healing, osteoporosis, arthritis, soft tissue calcification
Protease-activatable	IVISense Pan Cathepsin 680	Lysosomal pan-cathepsin activity	Cancer, arthritis, pulmonary neutrophilia/eosinophilia, atherosclerosis, general acute/chronic inflammation
	IVISense Pan Cathepsin 750 FAST	FAST version of Pan-Cathepsin, with faster kinetics and a broader imaging window	
	IVISense Cat B 680 FAST	Lysosomal cathepsin B activity	
	IVISense Cat K 680 FAST	Cathepsin K activity	Osteoclastic bone resorption, osteoporosis, soft tissue calcification, tumor-associated macrophages
	IVISense Neutrophil Elastase 680 FAST	Secreted neutrophil elastase activity	Pulmonary inflammation, acute neutrophilia, arthritis
	IVISense MMP 680	Secreted and membrane pan-matrix metalloprotease activity	Cancer, arthritis, pulmonary neutrophilia/eosinophilia, atherosclerosis, general acute/chronic inflammation

Note: The 680 and 750 indicate the emission wavelength of the fluorescent probe

Compliance with Ethical Standards Funding/Conflict of Interest: This work is sponsored by PerkinElmer Inc., and its R&D research division for developing advanced molecular imaging technologies. Both authors of this chapter (J.C. Tseng and J.D. Peterson) are employees of PerkinElmer Inc.

Ethical Approval: All animal research involved in this work followed the guidelines of PerkinElmer's Institutional Animal Care and Use Committee (IACUC). A research protocol (#01-0112) was approved for this study.

References

1. Medzhitov R. Origin and physiological roles of inflammation. Nature. 2008;454:428–35. https://doi.org/10.1038/nature07201.
2. Greten FR, Grivennikov SI. Inflammation and cancer: triggers, mechanisms, and consequences. Immunity. 2019;51:27–41. https://doi.org/10.1016/j.immuni.2019.06.025.
3. Fakhoury M. Inflammation in Alzheimer's disease. Curr Alzheimer Res. 2021;17:959–61. https://doi.org/10.2174/1567205017112101011105 13.
4. Roh JS, Sohn DH. Damage-associated molecular patterns in inflammatory diseases. Immune Netw. 2018:18. https://doi.org/10.4110/in.2018.18.e27.
5. Jones HR, Robb CT, Perretti M, Rossi AG. The role of neutrophils in inflammation resolution. Semin Immunol. 2016;28:137–45. https://doi.org/10.1016/j.smim.2016.03.007.
6. Martinez FO, Gordon S, Locati M, Mantovani A. Transcriptional profiling of the human monocyte-to-macrophage differentiation and polarization: new molecules and patterns of gene expression. J Immunol. 2006;177:7303–11. https://doi.org/10.4049/jimmunol.177.10.7303.
7. Tang T, Scambler TE, Smallie T, Cunliffe HE, Ross EA, Rosner DR, et al. Macrophage responses to lipopolysaccharide are modulated by a feedback loop involving prostaglandin E2, dual specificity phosphatase 1 and tristetraprolin. Sci Rep. 2017;7:4350. https://doi.org/10.1038/s41598-017-04100-1.
8. Zarghi A, Arfaei S. Selective COX-2 inhibitors: a review of their structure-activity relationships. Iran J Pharm Res. 2011;10:655–83.
9. Yi Y-S. Folate receptor-targeted diagnostics and therapeutics for inflammatory diseases. Immune Netw. 2016;16:337. https://doi.org/10.4110/in.2016.16.6.337.
10. Antonov AS, Antonova GN, Munn DH, Mivechi N, Lucas R, Catravas JD, et al. αVβ3 integrin regulates macrophage inflammatory responses via PI3 kinase/Akt-dependent NF-κB activation. J Cell Physiol. 2011;226:469–76. https://doi.org/10.1002/jcp.22356.
11. Mezu-Ndubuisi OJ, Maheshwari A. The role of integrins in inflammation and angiogenesis. Pediatr Res. 2021;89:1619–26. https://doi.org/10.1038/s41390-020-01177-9.
12. Dai R, Wu Z, Chu HY, Lu J, Lyu A, Liu J, et al. Cathepsin K: the action in and beyond bone. Front Cell Dev Biol. 2020:8. https://doi.org/10.3389/fcell.2020.00433.
13. Page-McCaw A, Ewald AJ, Werb Z. Matrix metalloproteinases and the regulation of tissue remodelling. Nat Rev Mol Cell Biol. 2007;8:221–33. https://doi.org/10.1038/nrm2125.
14. Canton J. Phagosome maturation in polarized macrophages. J Leukoc Biol. 2014;96:729–38. https://doi.org/10.1189/jlb.1MR0114-021R.
15. Bedard K, Krause K-H. The NOX family of ROS-generating NADPH oxidases: physiology and pathophysiology. Physiol Rev. 2007;87:245–313. https://doi.org/10.1152/physrev.00044.2005.
16. El-Benna J, Hurtado-Nedelec M, Marzaioli V, Marie J-C, Gougerot-Pocidalo M-A, Dang PM-C. Priming of the neutrophil respiratory burst: role in host defense and inflammation. Immunol Rev. 2016;273:180–93. https://doi.org/10.1111/imr.12447.
17. Stasia MJ. CYBA encoding p22phox, the cytochrome b558 alpha polypeptide: gene structure, expression, role and physiopathology. Gene. 2016;586:27–35. https://doi.org/10.1016/j.gene.2016.03.050.
18. Davies MJ, Hawkins CL. The role of myeloperoxidase in biomolecule modification, chronic inflammation, and disease. Antioxid Redox Signal. 2020;32:957–81. https://doi.org/10.1089/ars.2020.8030.

19. Jiang F, Zhang Y, Dusting GJ. NADPH oxidase-mediated redox Signaling: roles in cellular stress response, stress tolerance, and tissue repair. Sibley DR, editor. Pharmacol Rev. 2011;63: 218–42. https://doi.org/10.1124/pr.110.002980.
20. Fuhrman B, Shiner M, Volkova N, Aviram M. Cell-induced copper ion-mediated low density lipoprotein oxidation increases during in vivo monocyte-to-macrophage differentiation. Free Radic Biol Med. 2004;37:259–71. https://doi.org/10.1016/j.freeradbiomed.2004.04.026.
21. Ejlerskov P, Christensen DP, Beyaie D, Burritt JB, Paclet M-H, Gorlach A, et al. NADPH oxidase is internalized by Clathrin-coated pits and localizes to a Rab27A/B GTPase-regulated secretory compartment in activated macrophages. J Biol Chem. 2012;287:4835–52. https://doi.org/10.1074/jbc.M111.293696.
22. Kumar AP, Piedrafita FJ, Reynolds WF. Peroxisome proliferator-activated receptor γ ligands regulate myeloperoxidase expression in macrophages by an estrogen-dependent mechanism involving the -463GA promoter polymorphism. J Biol Chem. 2004;279:8300–15. https://doi.org/10.1074/jbc.M311625200.
23. Stapels DA, Geisbrecht BV, Rooijakkers SH. Neutrophil serine proteases in antibacterial defense. Curr Opin Microbiol. 2015;23:42–8. https://doi.org/10.1016/j.mib.2014.11.002.
24. Chua F, Laurent GJ. Neutrophil elastase: mediator of extracellular matrix destruction and accumulation. Proc Am Thorac Soc. 2006;3:424–7. https://doi.org/10.1513/pats.200603-078AW.
25. Garratt LW, Sutanto EN, Ling K-M, Looi K, Iosifidis T, Martinovich KM, et al. Matrix metalloproteinase activation by free neutrophil elastase contributes to bronchiectasis progression in early cystic fibrosis. Eur Respir J. 2015;46:384–94. https://doi.org/10.1183/09031936.00212114.
26. Elkington PT, Green JA, Friedland JS. Analysis of matrix metalloproteinase secretion by macrophages. 2009. p. 253–65. doi:https://doi.org/10.1007/978-1-59745-396-7_16.
27. Krotova K, Khodayari N, Oshins R, Aslanidi G, Brantly ML. Neutrophil elastase promotes macrophage cell adhesion and cytokine production through the integrin-Src kinases pathway. Sci Rep. 2020;10:15874. https://doi.org/10.1038/s41598-020-72667-3.
28. Laronha H, Caldeira J. Structure and function of human matrix metalloproteinases. Cell. 2020;9:1076. https://doi.org/10.3390/cells9051076.
29. Li H, Qiu Z, Li F, Wang C. The relationship between MMP-2 and MMP-9 expression levels with breast cancer incidence and prognosis. Oncol Lett. 2017; https://doi.org/10.3892/ol.2017.6924.
30. Burrage PS, Mix KS, Brinckerhoff CE. Matrix metalloproteinases: role in arthritis. Front Biosci. 2006;11:529. https://doi.org/10.2741/1817.
31. Yadati T, Houben T, Bitorina A, Shiri-Sverdlov R. The ins and outs of cathepsins: physiological function and role in disease management. Cell. 2020;9:1679. https://doi.org/10.3390/cells9071679.
32. Conus S, Simon H. Cathepsins and their involvement in immune responses. Swiss Med Wkly. 2010; https://doi.org/10.4414/smw.2010.13042.
33. Szulc-Dąbrowska L, Bossowska-Nowicka M, Struzik J, Toka FN. Cathepsins in bacteria-macrophage interaction: defenders or victims of circumstance? Front Cell Infect Microbiol. 2020:10. https://doi.org/10.3389/fcimb.2020.601072.
34. Jakoš T, Pišlar A, Jewett A, Kos J. Cysteine cathepsins in tumor-associated immune cells. Front Immunol. 2019:10. https://doi.org/10.3389/fimmu.2019.02037.
35. Fuchs N, Meta M, Schuppan D, Nuhn L, Schirmeister T. Novel opportunities for cathepsin S inhibitors in cancer immunotherapy by nanocarrier-mediated delivery. Cell. 2020;9:2021. https://doi.org/10.3390/cells9092021.
36. Montague-Cardoso K, Malcangio M. Cathepsin S as a potential therapeutic target for chronic pain. Med Drug Discov. 2020;7:100047. https://doi.org/10.1016/j.medidd.2020.100047.
37. Ntziachristos V, Ripoll J, Wang LV, Weissleder R. Looking and listening to light: the evolution of whole-body photonic imaging. Nat Biotechnol. 2005;23:313–20. https://doi.org/10.1038/nbt1074.

38. Roda A, Pasini P, Mirasoli M, Michelini E, Guardigli M. Biotechnological applications of bioluminescence and chemiluminescence. Trends Biotechnol. 2004;22:295–303. https://doi.org/10.1016/j.tibtech.2004.03.011.
39. Ntziachristos V, Bremer C, Weissleder R. Fluorescence imaging with near-infrared light: new technological advances that enable in vivo molecular imaging. Eur Radiol. 2003;13:195–208. https://doi.org/10.1007/s00330-002-1524-x.
40. Li S, Ruan Z, Zhang H, Xu H. Recent achievements of bioluminescence imaging based on firefly luciferin-luciferase system. Eur J Med Chem. 2021;211:113111. https://doi.org/10.1016/j.ejmech.2020.113111.
41. Contag CH, Bachmann MH. Advances in in vivo bioluminescence imaging of gene expression. Annu Rev Biomed Eng. 2002;4:235–60. https://doi.org/10.1146/annurev.bioeng.4.111901.093336.
42. Mezzanotte L, van 't Root M, Karatas H, Goun EA, CWGM L. In vivo molecular bioluminescence imaging: new tools and applications. Trends Biotechnol. 2017;35:640–52. https://doi.org/10.1016/j.tibtech.2017.03.012.
43. Zambito G, Chawda C, Mezzanotte L. Emerging tools for bioluminescence imaging. Curr Opin Chem Biol. 2021;63:86–94. https://doi.org/10.1016/j.cbpa.2021.02.005.
44. Dikalov S, Griendling KK, Harrison DG. Measurement of reactive oxygen species in cardiovascular studies. Hypertension. 2007;49:717–27. https://doi.org/10.1161/01.HYP.0000258594.87211.6b.
45. Bancirova M. Sodium azide as a specific quencher of singlet oxygen during chemiluminescent detection by luminol and Cypridina luciferin analogues. Luminescence. 2011;26:685–8. https://doi.org/10.1002/bio.1296.
46. Gross S, Gammon ST, Moss BL, Rauch D, Harding J, Heinecke JW, et al. Bioluminescence imaging of myeloperoxidase activity in vivo. Nat Med. 2009;15:455–61. https://doi.org/10.1038/nm.1886.
47. Kielland A, Blom T, Nandakumar KS, Holmdahl R, Blomhoff R, Carlsen H. In vivo imaging of reactive oxygen and nitrogen species in inflammation using the luminescent probe L-012. Free Radic Biol Med. 2009;47:760–6. https://doi.org/10.1016/j.freeradbiomed.2009.06.013.
48. Zhou J, Tsai Y-T, Weng H, Tang L. Noninvasive assessment of localized inflammatory responses. Free Radic Biol Med. 2012;52:218–26. https://doi.org/10.1016/j.freeradbiomed.2011.10.452.
49. Tseng J-C, Kung AL. In vivo imaging of inflammatory phagocytes. Chem Biol. 2012;19:1199–209. https://doi.org/10.1016/j.chembiol.2012.08.007.
50. Okajima T, Ohsaka T. Chemiluminescence of lucigenin by electrogenerated superoxide ions in aqueous solutions. Luminescence. 2003;18:49–57. https://doi.org/10.1002/bio.706.
51. Rezende F, Prior K-K, Löwe O, Wittig I, Strecker V, Moll F, et al. Cytochrome P450 enzymes but not NADPH oxidases are the source of the NADPH-dependent lucigenin chemiluminescence in membrane assays. Free Radic Biol Med. 2017;102:57–66. https://doi.org/10.1016/j.freeradbiomed.2016.11.019.
52. Shuhendler AJ, Pu K, Cui L, Uetrecht JP, Rao J. Real-time imaging of oxidative and nitrosative stress in the liver of live animals for drug-toxicity testing. Nat Biotechnol. 2014;32:373–80. https://doi.org/10.1038/nbt.2838.
53. Pfleger KDG, Eidne KA. Illuminating insights into protein-protein interactions using bioluminescence resonance energy transfer (BRET). Nat Methods. 2006;3:165–74. https://doi.org/10.1038/nmeth841.
54. Eglen RM, Reisine T, Roby P, Rouleau N, Illy C, Bossé R, et al. The use of AlphaScreen technology in HTS: current status. Curr Chem Genomics. 2008;1:2–10. https://doi.org/10.2174/1875397300801010002.
55. Zhang N, Francis KP, Prakash A, Ansaldi D. Enhanced detection of myeloperoxidase activity in deep tissues through luminescent excitation of near-infrared nanoparticles. Nat Med. 2013;19:500–5. https://doi.org/10.1038/nm.3110.

56. Hoshyar N, Gray S, Han H, Bao G. The effect of nanoparticle size on in vivo pharmacokinetics and cellular interaction. Nanomedicine. 2016;11:673–92. https://doi.org/10.2217/nnm.16.5.
57. Dragulescu-Andrasi A, Chan CT, De A, Massoud TF, Gambhir SS. Bioluminescence resonance energy transfer (BRET) imaging of protein–protein interactions within deep tissues of living subjects. Proc Natl Acad Sci. 2011;108:12060–5. https://doi.org/10.1073/pnas.1100923108.
58. Bhuckory S, Kays JC, Dennis AM. In vivo biosensing using resonance energy transfer. Biosensors. 2019;9:76. https://doi.org/10.3390/bios9020076.
59. So M-K, Xu C, Loening AM, Gambhir SS, Rao J. Self-illuminating quantum dot conjugates for in vivo imaging. Nat Biotechnol. 2006;24:339–43. https://doi.org/10.1038/nbt1188.
60. Xiong L, Shuhendler AJ, Rao J. Self-luminescing BRET-FRET near-infrared dots for in vivo lymph-node mapping and tumour imaging. Nat Commun. 2012;3:1193. https://doi.org/10.1038/ncomms2197.
61. Augusto FA, de Souza GA, de Souza Júnior SP, Khalid M, Baader WJ. Efficiency of electron transfer initiated chemiluminescence. Photochem Photobiol. 2013;89:1299–317. https://doi.org/10.1111/php.12102.
62. Rauhut MM. Chemiluminescence from concerted peroxide decomposition reactions. Acc Chem Res. 1969;2:80–7. https://doi.org/10.1021/ar50015a003.
63. Rauhut MM, Bollyky LJ, Roberts BG, Loy M, Whitman RH, Iannotta AV, et al. Chemiluminescence from reactions of electronegatively substituted aryl oxalates with hydrogen peroxide and fluorescent compounds. J Am Chem Soc. 1967;89:6515–22. https://doi.org/10.1021/ja01001a025.
64. Freeman R, Liu X, Willner I. Chemiluminescent and chemiluminescence resonance energy transfer (CRET) detection of DNA, metal ions, and aptamer–substrate complexes using Hemin/G-quadruplexes and CdSe/ZnS quantum dots. J Am Chem Soc. 2011;133:11597–604. https://doi.org/10.1021/ja202639m.
65. Lee D, Khaja S, Velasquez-Castano JC, Dasari M, Sun C, Petros J, et al. In vivo imaging of hydrogen peroxide with chemiluminescent nanoparticles. Nat Mater. 2007;6:765–9. https://doi.org/10.1038/nmat1983.
66. Bag S, Tseng J-C, Rochford J. A BODIPY-luminol chemiluminescent resonance energy-transfer (CRET) cassette for imaging of cellular superoxide. Org Biomol Chem. 2015;13:1763–7. https://doi.org/10.1039/C4OB02413C.
67. Kambayashi Y, Ogino K. Reestimation of Cypridina Luciferin Analogs (MCLA) as a chemiluminescence probe to detect active oxygen species—cautionary note for use of MCLA. J Toxicol Sci. 2003;28:139–48. https://doi.org/10.2131/jts.28.139.
68. Tseng J-C, Bailey D, Tupper T, Kung AL. Using glow stick chemistry for biological imaging. Mol Imaging Biol. 2014;16:478–87. https://doi.org/10.1007/s11307-014-0721-8.
69. Tseng J-C, Kung AL. In vivo imaging of endogenous enzyme activities using luminescent 1,2-dioxetane compounds. J Biomed Sci. 2015;22:45. https://doi.org/10.1186/s12929-015-0155-x.
70. Leblond F, Davis SC, Valdés PA, Pogue BW. Pre-clinical whole-body fluorescence imaging: review of instruments, methods and applications. J Photochem Photobiol B Biol. 2010;98:77–94. https://doi.org/10.1016/j.jphotobiol.2009.11.007.
71. Maeda H, Matsumura Y. EPR effect based drug design and clinical outlook for enhanced cancer chemotherapy. Adv Drug Deliv Rev. 2011;63:129–30. https://doi.org/10.1016/j.addr.2010.05.001.
72. Eaton VL, Vasquez KO, Goings GE, Hunter ZN, Peterson JD, Miller SD. Optical tomographic imaging of near infrared imaging agents quantifies disease severity and immunomodulation of experimental autoimmune encephalomyelitis in vivo. J Neuroinflammation. 2013;10:904. https://doi.org/10.1186/1742-2094-10-138.
73. Buono C, Anzinger JJ, Amar M, Kruth HS. Fluorescent pegylated nanoparticles demonstrate fluid-phase pinocytosis by macrophages in mouse atherosclerotic lesions. J Clin Invest. 2009;119:1373–81. https://doi.org/10.1172/JCI35548.

74. Uddin MJ, Crews BC, Blobaum AL, Kingsley PJ, Gorden DL, McIntyre JO, et al. Selective visualization of cyclooxygenase-2 in inflammation and cancer by targeted fluorescent imaging agents. Cancer Res. 2010;70:3618–27. https://doi.org/10.1158/0008-5472.CAN-09-2664.
75. Han W, Zaynagetdinov R, Yull FE, Polosukhin VV, Gleaves LA, Tanjore H, et al. Molecular imaging of folate receptor β–positive macrophages during acute lung inflammation. Am J Respir Cell Mol Biol. 2015;53:50–9. https://doi.org/10.1165/rcmb.2014-0289OC.
76. Chen W-T, Mahmood U, Weissleder R, Tung C-H. Arthritis imaging using a near-infrared fluorescence folate-targeted probe. Arthritis Res Ther. 2005;7:R310–7. https://doi.org/10.1186/ar1483.
77. Bridgewater RE, Norman JC, Caswell PT. Integrin trafficking at a glance. J Cell Sci. 2012;125:3695–701. https://doi.org/10.1242/jcs.095810.
78. Paul NR, Jacquemet G, Caswell PT. Endocytic trafficking of integrins in cell migration. Curr Biol. 2015;25:R1092–105. https://doi.org/10.1016/j.cub.2015.09.049.
79. Moreno-Layseca P, Icha J, Hamidi H, Ivaska J. Integrin trafficking in cells and tissues. Nat Cell Biol. 2019;21:122–32. https://doi.org/10.1038/s41556-018-0223-z.
80. Su G, Atakilit A, Li JT, Wu N, Bhattacharya M, Zhu J, et al. Absence of integrin αvβ3 enhances vascular leak in mice by inhibiting endothelial cortical actin formation. Am J Respir Crit Care Med. 2012;185:58–66. https://doi.org/10.1164/rccm.201108-1381OC.
81. Laitinen I, Saraste A, Weidl E, Poethko T, Weber AW, Nekolla SG, et al. Evaluation of αvβ3 integrin-targeted positron emission tomography tracer 18 F-Galacto-RGD for imaging of vascular inflammation in atherosclerotic mice. Circ Cardiovasc Imaging. 2009;2:331–8. https://doi.org/10.1161/CIRCIMAGING.108.846865.
82. Jenkins WS, Vesey AT, Vickers A, Neale A, Moles C, Connell M, et al. In vivo alpha-V beta-3 integrin expression in human aortic atherosclerosis. Heart. 2019;105:1868–75. https://doi.org/10.1136/heartjnl-2019-315103.
83. Razavian M, Marfatia R, Mongue-Din H, Tavakoli S, Sinusas AJ, Zhang J, et al. Integrin-targeted imaging of inflammation in vascular remodeling. Arterioscler Thromb Vasc Biol. 2011;31:2820–6. https://doi.org/10.1161/ATVBAHA.111.231654.
84. Ludwig BS, Kessler H, Kossatz S, Reuning U. RGD-binding integrins revisited: how recently discovered functions and novel synthetic ligands (re-)shape an ever-evolving field. Cancers (Basel). 2021;13:1711. https://doi.org/10.3390/cancers13071711.
85. Lin S-A, Patel M, Suresch D, Connolly B, Bao B, Groves K, et al. Quantitative longitudinal imaging of vascular inflammation and treatment by ezetimibe in apoE mice by FMT using new optical imaging biomarkers of cathepsin activity and αvβ3 integrin. Int J Mol Imaging. 2012;2012:1–13. https://doi.org/10.1155/2012/189254.
86. Wu L, Sedgwick AC, Sun X, Bull SD, He X-P, James TD. Reaction-based fluorescent probes for the detection and imaging of reactive oxygen, nitrogen, and sulfur species. Acc Chem Res. 2019;52:2582–97. https://doi.org/10.1021/acs.accounts.9b00302.
87. Driever SM, Fryer MJ, Mullineaux PM, Baker NR. Imaging of reactive oxygen species in vivo. In: Pfannschmidt T, editor. Plant signal transduct. Totowa, NJ: Humana Press; 2009. p. 109–16. https://doi.org/10.1007/978-1-59745-289-2_7.
88. Kundu K, Knight SF, Willett N, Lee S, Taylor WR, Murthy N. Hydrocyanines: a class of fluorescent sensors that can image reactive oxygen species in cell culture, tissue, and in vivo. Angew Chemie Int Ed. 2009;48:299–303. https://doi.org/10.1002/anie.200804851.
89. Prunty MC, Aung MH, Hanif AM, Allen RS, Chrenek MA, Boatright JH, et al. In vivo imaging of retinal oxidative stress using a reactive oxygen species–activated fluorescent probe. Investig Opthalmol Vis Sci. 2015;56:5862. https://doi.org/10.1167/iovs.15-16810.
90. Ito R, Kamiya M, Urano Y. Molecular probes for fluorescence image-guided cancer surgery. Curr Opin Chem Biol. 2022;67:102112. https://doi.org/10.1016/j.cbpa.2021.102112.
91. Suri S, Lehman SM, Selvam S, Reddie K, Maity S, Murthy N, et al. In vivo fluorescence imaging of biomaterial-associated inflammation and infection in a minimally invasive manner. J Biomed Mater Res Part A. 2015;103:76–83. https://doi.org/10.1002/jbm.a.35162.

92. Uusitalo LM, Hempel N. Recent advances in intracellular and in vivo ROS sensing: focus on nanoparticle and nanotube applications. Int J Mol Sci. 2012;13:10660–79. https://doi.org/10.3390/ijms130910660.
93. Wu L, Wu I-C, DuFort CC, Carlson MA, Wu X, Chen L, et al. Photostable Ratiometric Pdot probe for in vitro and in vivo imaging of hypochlorous acid. J Am Chem Soc. 2017;139:6911–8. https://doi.org/10.1021/jacs.7b01545.
94. Funovics M, Weissleder R, Tung C-H. Protease sensors for bioimaging. Anal Bioanal Chem. 2003;377:956–63. https://doi.org/10.1007/s00216-003-2199-0.
95. Weissleder R, Tung C-H, Mahmood U, Bogdanov A. In vivo imaging of tumors with protease-activated near-infrared fluorescent probes. Nat Biotechnol. 1999;17:375–8. https://doi.org/10.1038/7933.
96. Wunder A, Tung C-H, Müller-Ladner U, Weissleder R, Mahmood U. In vivo imaging of protease activity in arthritis: a novel approach for monitoring treatment response. Arthritis Rheum. 2004;50:2459–65. https://doi.org/10.1002/art.20379.
97. Kossodo S, Zhang J, Groves K, Cuneo GJ, Handy E, Morin J, et al. Noninvasive in vivo quantification of neutrophil elastase activity in acute experimental mouse lung injury. Int J Mol Imaging. 2011;2011:1–11. https://doi.org/10.1155/2011/581406.
98. Akers WJ, Xu B, Lee H, Sudlow GP, Fields GB, Achilefu S, et al. Detection of MMP-2 and MMP-9 activity in vivo with a triple-helical peptide optical probe. Bioconjug Chem. 2012;23:656–63. https://doi.org/10.1021/bc300027y.
99. Chen X, Lee D, Yu S, Kim G, Lee S, Cho Y, et al. In vivo near-infrared imaging and phototherapy of tumors using a cathepsin B-activated fluorescent probe. Biomaterials. 2017;122:130–40. https://doi.org/10.1016/j.biomaterials.2017.01.020.
100. Glinzer A, Ma X, Prakash J, Kimm MA, Lohöfer F, Kosanke K, et al. Targeting elastase for molecular imaging of early atherosclerotic lesions. Arterioscler Thromb Vasc Biol. 2017;37:525–33. https://doi.org/10.1161/ATVBAHA.116.308726.
101. Korideck H, Peterson JD. Noninvasive quantitative tomography of the therapeutic response to dexamethasone in ovalbumin-induced murine asthma. J Pharmacol Exp Ther. 2009;329:882–9. https://doi.org/10.1124/jpet.108.147579.
102. Ibarra JM, Jimenez F, Martinez HG, Clark K, Ahuja SS. MMP-activated fluorescence imaging detects early joint inflammation in collagen-antibody-induced arthritis in CC-chemokine Receptor-2-null mice, in-vivo. Int J Inflam. 2011;2011:1–6. https://doi.org/10.4061/2011/691587.
103. Peterson JD, LaBranche TP, Vasquez KO, Kossodo S, Melton M, Rader R, et al. Optical tomographic imaging discriminates between disease-modifying anti-rheumatic drug (DMARD) and non-DMARD efficacy in collagen antibody-induced arthritis. Arthritis Res Ther. 2010;12:R105. https://doi.org/10.1186/ar3038.